https://doi.org/10.5194/egusphere-2025-4348
Preprint. Discussion started: 25 September 2025

Historical and future changes and present-day uncertainties of ozone in China from CMIP6 models

Shuai Li[1], Hua Zhang[2*], Qi Chen[3], Yonghang Chen[1], Qi An[4], Zhili Wang[2, 5], Xinping Wu[6]

[1] College of Environmental Science and Engineering, Donghua University, Shanghai 201620, China
[2] State Key Laboratory of Severe Weather, Chinese Academy of Meteorological Sciences, Beijing 100081, China
[3] CMA earth system modeling and prediciton center, Beijing 100081, China
[4] Meteorological Service Center for the Core Areas of the Capital, Beijing 100081, China
[5] Key Laboratory of Atmospheric Chemistry of CMA, Chinese Academy of Meteorological Sciences, Beijing 100081, China
[6] Tazhong Meteorological Station, Qiemo, Xinjiang, China

Correspondence: Hua Zhang (huazhang@cma.gov.cn)

Abstract: Ozone (O_3) contributes to global climate change and poses a direct threat to human health. This study analyzes historical and future changes, as well as current uncertainties, in surface O_3 concentrations in China, based on CMIP6 and the Tracking Air Pollution in China (TAP) dataset. The results are as follows: (1) The Multi-Model Ensemble Mean (MME) of CMIP6 simulated O_3 concentrations is higher during June–August (JJA), averaging 105 $\mu g \cdot m^{-3}$, and lowest during December–February (DJF) at 55 $\mu g \cdot m^{-3}$. (2) CMIP6 models generally underestimate O_3 concentrations in most regions of China, with the most significant underestimation occurring in East China. (3) The MME-simulated O_3 concentrations exhibit lower Bias, MAE, and RMSE over natural land surfaces compared to those over anthropogenic land surfaces. The Bias reaches its minimum under cloudy conditions and peaks under partly cloudy conditions. Furthermore, the Bias generally increases with rising $PM_{2.5}$ concentrations, however, once $PM_{2.5}$ exceeds a specific threshold, the Bias begins to decline. (4) Over the entire historical period, the MME simulates an increase of 39.3 $\mu g \cdot m^{-3}$ in the annual mean surface O_3 concentration in China. (5) Under future SSP scenarios, MME projects generally increasing O_3 under weak mitigation (SSP3-7.0), with East China rising by 26.9%. Strong mitigation (SSP1-2.6) leads to widespread decreases, especially in Southwest and South China (>30 $\mu g \cdot m^{-3}$). (6) Differences in climate treatment, circulation, chemistry, and precursor emissions create substantial uncertainties, emphasizing the need to understand how emissions (including precursors and $PM_{2.5}$), climate, and model processes jointly affect future O_3 projections.

1 Introduction

Ozone (O_3) is one of the most important trace components in the Earth's atmosphere, serving as a protective barrier for the global ecosystem and a crucial heat source in the stratosphere (Zhang et al., 2017), and its variations strongly influence the climate of the stratosphere and even the troposphere (Xie et al., 2017; Haase and Matthes, 2019; Lin and Ming, 2021), playing a critical role in controlling the temperature structure of Earth's atmosphere. Studies have shown that 90% of atmospheric O_3 is concentrated in the stratosphere, with only about 10% distributed in the troposphere, however, the climatic effects caused by tropospheric O_3 variations can be comparable to the perturbations induced in the stratosphere (Xie and Zhang, 2014). As one of the major sources of OH radicals, O_3 indirectly determines the lifetime of various trace constituents in the troposphere (Levy, 1971). Additionally, O_3 is an important greenhouse gas, a strong oxidant, and a plant toxin, which not only influences global climate change (Monks et al., 2015) but also directly harms human health (Shindell et al., 2012; Wang et al., 2021) and vegetation growth (Avnery et al., 2011; Lin et al., 2018; Feng et al., 2018). The Global Burden of Disease Report (GBDR) states that more than 360,000 premature deaths globally in 2019 were attributed to exposure to ambient O_3, and that high O_3 exposure may exacerbate the $PM_{2.5}$-mortality risk (Weichenthal et al., 2017). Therefore, studying the evolution of O_3 is of great significance for understanding global climate change and protecting Earth's organisms.

Over the past few years, due to rapid industrial development, precursor pollutants have been continuously emitted in large quantities, causing severe $PM_{2.5}$ and O_3 pollution in China (Maji et al., 2018; Lu et al., 2018; Qin et al., 2021). To improve air quality, the State Council issued the "Air Pollution Prevention and Control Action Plan" (APPCAP) in 2013, with the goal of reducing $PM_{2.5}$ concentrations in the key regions of Beijing-Tianjin-Hebei, the Yangtze River Delta, and the Pearl River Delta by 25%, 20%, and 15%, respectively, by 2017. Accordingly, a series of air pollution control measures have been implemented, including optimizing industrial structure, increasing the supply of clean energy, limiting high-emission vehicles, and banning high-emission sources such as open biomass burning (Qiu et al., 2016). As a result, since the "13th Five-Year Plan", China has made significant progress in air pollution mechanism research and control (Li et al., 2020; Lu et al., 2020; An et al., 2022; Su et al., 2022), particularly with a notable decrease in the annual average concentration of $PM_{2.5}$ in major regions.

In stark contrast to the improvements in $PM_{2.5}$ pollution control, most regions in China experienced a persistently fluctuating upward trend in annual O_3 concentrations during 2013–2018, with an average annual increase of 1–3 ppb (Li et al., 2019). By 2018, the national annual mean O_3 concentration had increased by 17.59% and 15.22% compared to 2013 and 2015 levels, respectively (Wang et al., 2020). The proportion of O_3-polluted days has become increasingly significant, and prolonged, large-scale O_3 pollution episodes have occurred more frequently, particularly in major urban agglomerations such as the Beijing-Tianjin-Hebei (BTH), Yangtze River Delta (YRD), and Pearl River Delta (PRD) regions (Dai et al., 2020; Zhao et al., 2020). Notably, since 2015 in the PRD and since 2017 in the YRD, the proportion of days with O_3 exceedance has surpassed that of particulate matter, making O_3 the primary pollutant (Lu et al., 2018; Wang et al., 2020). Despite the positive effects of policy implementation on reducing nitrogen oxides (NO_x) and volatile organic compounds (VOCs) in China (Lu et al., 2018), significant uncertainties remain regarding the abundance, spatial distribution, and related processes of these short-lived gases, which constrain the further optimization and effectiveness of emission control policies (Wild et al., 2020). Against this backdrop, surface O_3 pollution in China continues to worsen and expand. While $PM_{2.5}$ pollution has shown consistent improvement, effectively controlling O_3 pollution has emerged as a critical challenge for air quality management in China, posing serious difficulties for both the scientific community and policymakers. Under the guidance of the "Dual-Carbon" strategy, achieving sustained improvements in air quality through precise and science-based measures has become an urgent scientific and technological issue. Therefore, accurately understanding the spatiotemporal evolution of surface O_3 concentrations in China is of great importance.

Currently, ground-based observations (including surface and radiosonde measurements) (Zhan et al., 2021; Liu et al., 2022), satellite remote sensing retrievals (such as column concentrations, vertical profiles, and multi-source data fusion) (Hubert et al., 2021; Zhao et al., 2022), and model simulations (Xue et al., 2020; Morgenstern, 2021) provide essential data and analytical approaches for monitoring O_3 and its precursors, investigating pollution sources and transport characteristics, and evaluating the accuracy of retrieval products. Ground-based observations are known for their high accuracy, satellite remote sensing offers broad coverage, and model simulations can extend both spatially and temporally through parameterization, these methods complement each other and collectively support ozone-related research. For a long time, chemical-climate models have been essential tools for global surface O_3

https://doi.org/10.5194/egusphere-2025-4348
Preprint. Discussion started: 25 September 2025

research, capable of reproducing past and present O_3 distributions across different spatial and temporal scales, and exploring their relationships with precursors and atmospheric physical-dynamic processes. However, due to the complexity of the tropospheric O_3 budget mechanisms, particularly the effects of chemical reaction chains, precursor emission distributions, and meteorological conditions, significant discrepancies remain in model results, both among different models and compared with observations. These discrepancies reflect the limitations of the models in parameterization of physical and chemical processes, as well as uncertainties in emission inventories and boundary conditions. Therefore, identifying, investigating, and quantifying the differences between models and observations is crucial for improving and advancing model performance (Young et al., 2018).

CMIP6 and the latest IPCC AR6 adopt new emission scenarios driven by different socioeconomic pathways, the Shared Socioeconomic Pathways (SSPs), replacing the four Representative Concentration Pathways (RCPs) used in CMIP5, this is a significant advancement in the CMIP6 scenarios (Eyring et al., 2016; Zhou et al., 2019). Previous studies have shown that most CMIP6 Earth System Models (ESMs) are capable of capturing the spatial distribution of global surface O_3 concentrations (Turnock et al., 2020; Ivanciu et al., 2021; Griffiths et al., 2021; Shang et al., 2021), but they tend to produce an overall positive bias of 5–10% (3.6±4.4 ppbv) (Sun and Archibal, 2021), with larger biases in the Northern Hemisphere and smaller biases in the Southern Hemisphere. This discrepancy may be attributed to the limitations of O_3 precursor emission data (Young et al., 2013). Currently, the evaluation of the latest CMIP6 simulations for surface O_3 in China is still limited. Therefore, this paper based on multi-model O_3 products from CMIP6, conducts an analysis of the historical and future changes of surface O_3 in China, as well as the associated current uncertainties. First, using the O_3 dataset from the Tracking Air Pollution in China (TAP), we assess the distribution and uncertainty of surface O_3 simulated by nine CMIP6 models under various conditions, including different temperatures, cloud cover levels, complex land surface types, and pollutant concentrations, for the period 2014–2023 across China and its seven sub-regions (Northeast China, North China, East China, South China, Central China, Northwest China and Southwest China) (Figure 1). Secondly, the changes in surface O_3 over different regions of China during the historical period 1850–2014 are calculated to provide a background for the analysis of future changes. Then, based on different SSPs in CMIP6 experiments, the future changes in surface O_3 across China are predicted and analysed for the period 2015–2100. Finally, a comparison of different CMIP6 models under a single future scenario

(SSP3-7.0) is conducted to identify the potential causes of models differences, aiming to provide valuable references for future O3 pollution control and prediction efforts.

2 Research data and methods

The data used in this paper primarily includes O_3 products simulated by all models (9 models) in the CMIP6 chemistry models ("AERmon" CMIP6 table ID) under both historical and future scenarios (see Table 1). All data can be accessed from the World Climate Research Programme node(WCRP) (https://esgf-node.llnl.gov/search/cmip6/, last access: 8 April 2024). Specifically, all available data from 1850 to 2014 were obtained from the historical experiments of CMIP6 (Eyring et al., 2016), which studied the surface O_3 changes in China during the industrial period. Additionally, all available data for the period 2015–2100 from different shared economic pathways in ScenarioMIP (O'Neill et al., 2016), were used, and the specific SSP3-7.0-lowNTCF scenario from AerChemMIP (Collins et al., 2017) were used to investigate future changes in surface O_3 across different regions of China. To investigate the potential drivers behind the differences in future surface O_3 projections over China and its sub-regions under the SSP3-7.0 scenario, this study further incorporates and analyzes VOCs emission data provided by CMIP6. In CMIP6, variables representing non-methane volatile organic compound (NMVOC) emissions primarily include emivoc and emibvoc. The emivoc variable denotes the total emission rate of NMVOCs, covering both anthropogenic and biogenic sources, whereas emibvoc represents NMVOCs emissions from natural sources (e.g., vegetation), and is commonly used as a proxy for biogenic volatile organic compounds (BVOCs). For clarity and consistency, the terms NMVOCs and BVOCs are hereafter used to refer to the emission fluxes represented by emivoc and emibvoc, respectively.

For the historical experiments, CMIP6 provides O_3 data from 9 models and 44 ensemble members. The future scenario with the most available data is SSP3-7.0, with O_3 data from 9 models and 37 ensemble members. This is followed by SSP3-7.0-lowNTCF scenarios, which have O_3 data from 8 models and 15 ensemble members. For other scenarios from the Tier 1 experiments in CMIP6 (SSP1-2.6, SSP2-4.5), O_3 data from 5 models are available for analysis, while only 4 models are available for SSP5-8.5. Due to the limited availability of model data for the Tier 2 CMIP6 scenarios (SSP1-1.9, SSP4-3.4, SSP4-6.0, and SSP5-3.4-over), our analysis focuses on SSP3-7.0 and the other scenarios from the Tier 1 experiments.

Table1. Number of ensemble members used for the historical- and future-scenario experiments from each model in the analysis of surface O_3 in this study.

CMIP6 Models	**Institution**	**Historical**	**SSP1-2.6**	**SSP2-4.5**	**SSP3-7.0**	**SSP3-7.0-lowNTCF**	**SSP5-8.5**	**Model reference**
BCC-ESM1	Beijing Climate Center, China Meteorological Administration, China	3			3	3		Wu et al. (2020)
CESM2-WACCM	National Center for Atmospheric Research, Climate and Global Dynamics Laboratory, USA	3			3	3		Emmons et al. (2020)
EC-Earth3-AerChem	European Consortium of Meteorological Services, Research Institutes, and High-performance Computing Centers	4		1	3	3		Noije et al. (2021)
GFDL-ESM4	NOAA Geophysical Fluid Dynamics Laboratory, USA	1	1	1	1	1	1	Horowitz et al. (2020)
ISPL-CM5A2-INCA	Institute Pierre Simon Laplace, Paris, France	1			1	1		Sepulchre et al. (2020)
MIROC-ES2H	University of Tokyo, National Institute for Environmental Studies, and Japan Agency for Marine – Earth Science and Technology, Japan	3	1	2	1		3	Hajima et al. (2020)
MRI-ESM2-0	Meteorological Research Institute, Japan	10	4	10	5	3	5	Yukimoto et al. (2019)
UKESM1-0-LL	Natural Environment Research Council, and Met Office, United Kingdom	18	5	5	19	1	4	Sellar et al. (2019)
UKESM1-1-LL	Natural Environment Research Council, and Met Office, United Kingdom	1	3		1			Sellar et al. (2019)
Total number of models		44	14	19	37	15	13	

To assess the uncertainty in the CMIP6 simulation of current O_3 concentrations, this study utilizes the TAP (http://tapdata.org.cn/, last access: 8 April 2024) O_3 monthly products for the period from January 2014 to December 2023, with a spatial resolution of 0.1°. TAP is a near-real-time atmospheric composition tracking dataset for China, developed by Tsinghua University in collaboration with several other institutions, which mainly includes O_3, $PM_{2.5}$ and their major chemical components. The O_3 product is derived through a machine learning model that integrates multiple data sources, including O_3 observational data, satellite remote sensing vertical profiles of O_3, CMAQ simulations, WRF simulations, vegetation indices, nighttime lights, and population data, to estimate daily O_3 concentrations. TAP estimates show a high correlation with in-situ observations of maximum daily 8-hour average O_3, with an R^2 value of up to 0.70 (Xue et al., 2020; Xiao et al., 2022). Figure 1 shows the trends in surface pollutant concentrations across China and its sub-regions from 2000 to 2023 based on TAP data. Overall, O_3 concentrations have shown an increasing trend (10% increase) across China and sub-regions over the past decade, with a multi-year average concentration of 123.3 $\mu g \cdot m^{-3}$. Among these, North China exhibits the most significant increase (20% increase), with the highest average concentration of 141 μg·m^{-3}, followed by East China with 133 μg·m^{-3}, and the Northeast and Southwest regions have lower concentrations, with average values of 114 μg·m^{-3} and 106 μg·m^{-3}, respectively. In contrast, $PM_{2.5}$ concentrations have shown a decreasing trend (35% decrease) over the past 24 years, with a multi-year average concentration of 41 μg·m^{-3}. North China again shows the most notable decrease (42% decrease), with the highest average concentration of 57 μg·m^{-3}, followed by Central China at 54 μg·m^{-3}, and the Northwest and Southwest regions have lower concentrations, with averages of 32 μg·m^{-3} and 31 μg·m^{-3}, respectively. Except for the Northwest (2015), all other regions reached their peak concentrations in 2006–2007. The components of $PM_{2.5}$ have also shown decreasing trends, with the most significant reductions observed in SO_4 and OM, while the reductions in BC and NH_4 are less pronounced.

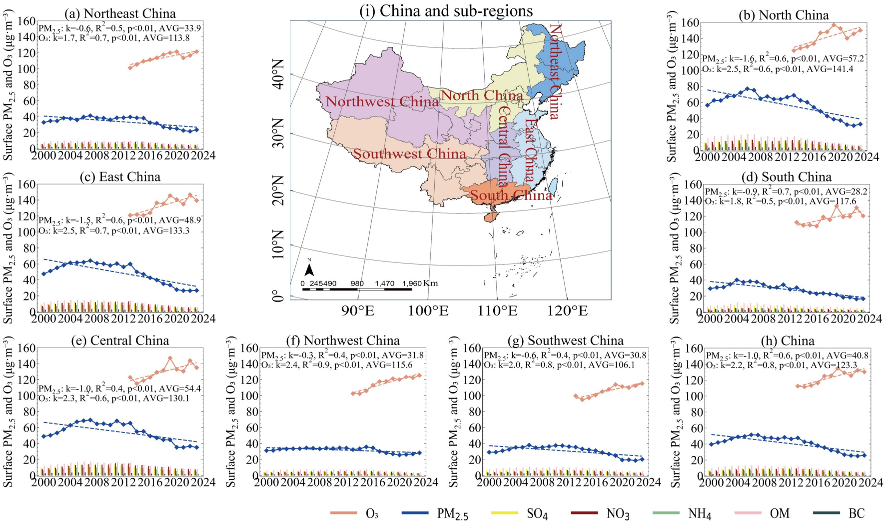

Figure 1. An overview of the geographic location of China and seven sub-regions (Northeast China, North China, East China, South China, Central China, Northwest China and Southwest China), and the annual variations in O_3 and $PM_{2.5}$ components from 2000–2023 based on TAP data.

In this paper, surface O_3 concentration is obtained by extracting the lowest vertical layer data from the horizontal and vertical grids of each CMIP6 model. For each model, the mean of all available ensemble products is taken as the model's simulation results. In assessing the uncertainty of CMIP6 simulations

https://doi.org/10.5194/egusphere-2025-4348
Preprint. Discussion started: 25 September 2025

for current O_3 concentrations, all CMIP6 data are linearly interpolated to a resolution of 0.1° to match the TAP data.

3 Present-Day O_3 concentrations simulations and uncertainties

3.1 Under different temperature and sub-regions

Temperature directly influences O_3 production by affecting the rates of photochemical reactions and the emission of plant VOCs, such as isoprene (Coates et al., 2016). Therefore, this study compares and analyzes the multi-year annual mean and seasonal distribution, standard deviation, and biases with TAP data for surface O_3 concentrations over China based on the Multi-Model Ensemble Mean (MME) of CMIP6 for the period 2014–2023 (Figure 2). It is evident that during summer (June, July, and August; JJA), MME shows higher O_3 concentrations, with a mean value of 105 $\mu g \cdot m^{-3}$. This is primarily due to increased photolysis activity, higher levels of oxidants, and enhanced biogenic emissions, all of which promote O_3 formation .Additionally, high temperatures are typically associated with increased atmospheric stability and a reduction in mixing layer height, making it more difficult for O_3 to disperse and dilute, leading to its accumulation near the surface and higher concentrations(Yang et al., 2022). In spring (March, April, and May; MAM) and autumn (September, October, and November; SON), the simulated O_3 concentrations are lower than in JJA, with mean values of 89 $\mu g \cdot m^{-3}$ and 78 $\mu g \cdot m^{-3}$, respectively. The lowest O_3 concentrations are observed in winter (December, January, and February; DJF), with a mean of 55 $\mu g \cdot m^{-3}$.

For the seven sub-regions, the seasonal patterns are generally consistent with those of the entire China (except for South China). Among them, Central China exhibits the highest O_3 concentration during JJA, reaching up to 117 $\mu g \cdot m^{-3}$, while the lowest concentration is simulated in DJF, at only 34 $\mu g \cdot m^{-3}$. In South China, O_3 concentrations are higher in SON, with a mean value of 99 $\mu g \cdot m^{-3}$, slightly exceeding those in JJA. According to TAP data, O_3 concentrations in JJA are also lower than those in MAM and SON in South China, and only slightly higher than in DJF. This could be attributed to the stronger southeast monsoon during JJA, which drives the northward transport of O_3 and its precursors, while also bringing increased precipitation and humidity (Yin et al., 2019), thereby reducing O_3 concentrations. In Southwest China, O_3 concentrations during MAM, SON, and DJF are notably higher than in other regions, particularly in the Tibetan Plateau, where the average O_3 concentration in DJF exceeds 90 μg·m^{-3}. This may result from transboundary transport from foreign regions, especially India, where precursor emissions and O_3 concentrations are relatively high (Sahu et al., 2021). In Northwest China, O_3 concentrations remain high across all four seasons, with the average O_3 concentrations in JJA reaching 113 μg·m^{-3}, and in MAM and DJF, O_3 concentrations are second only to those in Southwest China. Northeast China, on the other hand, has the lowest O_3 concentrations among all sub-regions, particularly during MAM, JJA, and SON, with concentrations of only 76 μg·m^{-3}, 88 μg·m^{-3}, and 54 μg·m^{-3}, respectively. In the experimental scenario designed by Zhang et al. (2018), which applied clean-air background concentration boundary conditions and excluded the influence of transboundary anthropogenic emissions from foreign regions, simulated O_3 concentrations decreased significantly over western China but showed little change over eastern China. These results suggest that emissions from external regions primarily affect O_3 levels in western China, whereas domestic emissions remain the dominant contributor to O_3 concentrations in eastern China.

The standard deviation (SD) among the models is largest in DJF (especially in the Sichuan Basin of Southwest China and South China), followed by JJA, smallest in SON. This suggests greater diversity in the seasonal O_3 cycles simulated by individual models during DJF, especially for UKESM1-0-LL and UKESM1-1-LL, which exhibit the most distinct seasonal cycles among the nine models (Figure 3), with significant negative biases in simulated O_3 concentrations during DJF. The spatial variation of the Bias of MME shows that O_3 concentrations are significantly underestimated in the eastern and northern China, particularly during DJF. In contrast, concentrations are overestimated in Southwest China, especially in SON and JJA. The bias in Northwest China is the lowest across all seasons, with simulated O_3 concentrations most closely matching the TAP values.

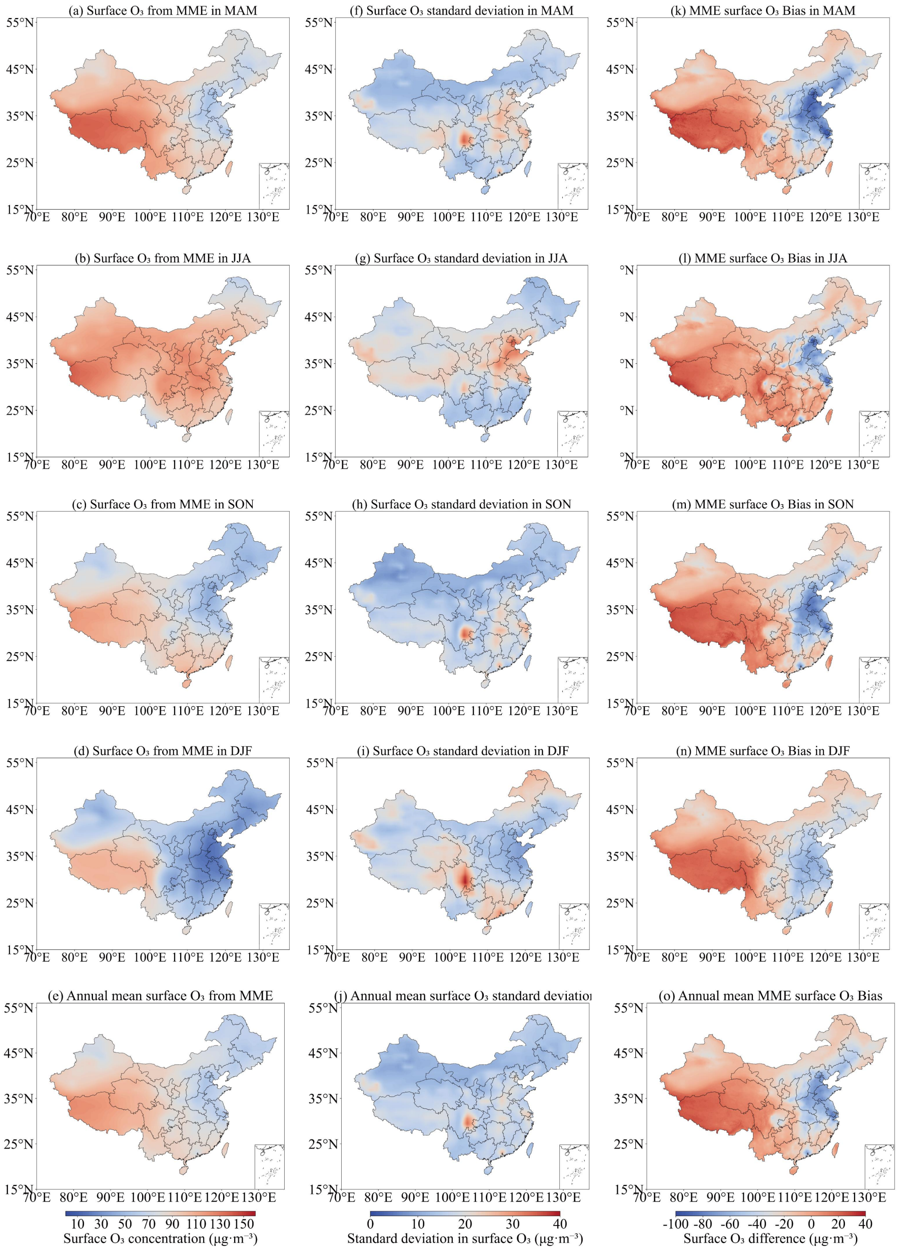

Figure 2. Multi-model (nine CMIP6 models) annual and seasonal mean surface O$_3$ concentrations over the 2014–2023 period in (a) MAM; (b) JJA; (c) SON; (d) DJF; and (e) annual mean. The SD of the MME in (f)MAM, (g) DJF, (h) JJA, (i)SON, and (j) annual mean. The difference between the MME and TAP observations in (k)MAM, (l) DJF, (m) JJA, (n)SON, and (o) annual mean.

The annual cycles of surface O_3 concentrations in China and its sub-regions simulated by the nine CMIP6 models were compared with the TAP-derived values (Figure 3), it can be seen that the correlation between the two is generally good in most regions ($r > 0.73$), which suggests that the seasonality of the circulation patterns, stratosphere-troposphere exchange, and natural emissions are well captured. However, (1) the timing of O_3 peak concentrations in the CMIP6 models (mostly in July–August) is slightly delayed compared to TAP (mostly in May–June), which is consistent with the results of the ACCMIP models (Young et al., 2018). (2) The nine CMIP6 models evaluated in this study exhibit significant underestimation of O_3 concentrations across most sub-regions of China, with the most severe underestimations found in UKESM1-0-LL and UKESM1-1-LL, except for slight overestimations in Southwest China from May to September, all other regions show underestimations, particularly in East and Central China during DJF, where the simulated O_3 concentrations are nearly 60 $\mu g \cdot m^{-3}$ lower than those calculated by TAP. This is consistent with the findings of Turnock et al. (2020), and may be due to excessive NO_x titration in the UKESM1-0-LL model, leading to an underestimation of surface O_3 concentrations over much of the Northern Hemisphere's continental regions during DJF. (3) In contrast, a small number of CMIP6 models evaluated in this study, including BCC-ESM1, EC-Earth3-AerChem, and MRI-ESM2-0, show a certain degree of overestimation in surface O_3 concentrations throughout the year in Southwest China (with an average overestimation of 30 $\mu g \cdot m^{-3}$), Northwest China (with an average overestimation of 10 $\mu g \cdot m^{-3}$), and during JJA in South China. This may result from common sources of error in the models, such as uncertainties in emission inventories, deposition processes, or vertical mixing (Wild et al., 2020). Additionally, the coarse resolution of ESMs may lead to overestimation of O_3 concentrations in polluted areas, while higher-resolution models and better consistency between nested models may improve the accuracy of simulated surface O_3 concentrations (Neal et al., 2017).

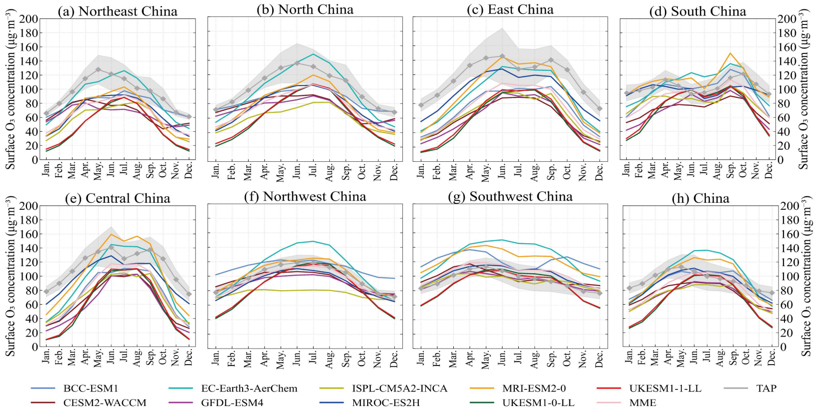

Figure 3. Comparison of the annual cycle of O_3 concentrations, between individual CMIP6 models, the MME and TAP in China and sub-regions for the period 2014–2023. The shading shows SD of TAP observations within the region.

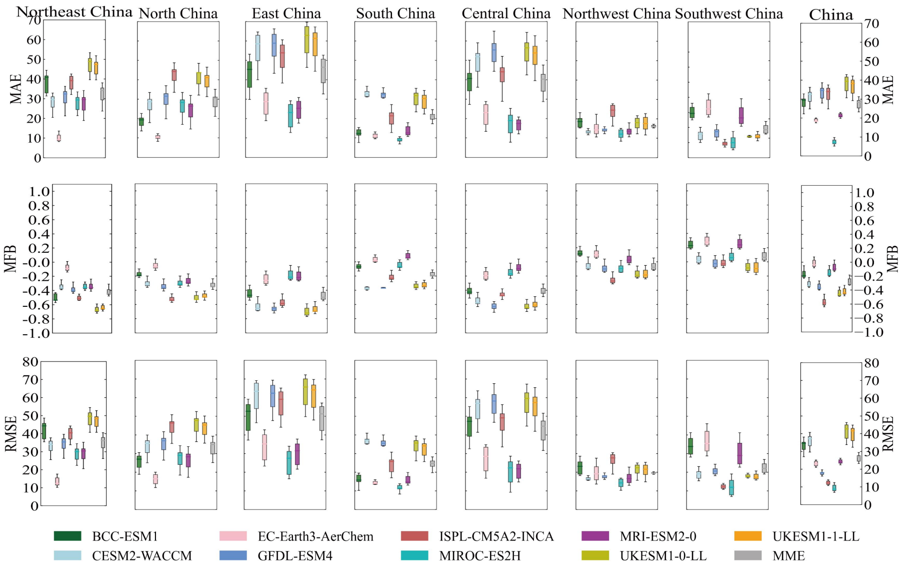

Figure 4. Distribution of differences for O_3 concentrations ($\mu g \cdot m^{-3}$) from nine CMIP6 models in China and sub-regions during 2014–2023. The box plots show the 25th and 75th percentiles as solid boxes, median values as solid lines, dots represent the concentrations from MAE, MFB and RMSE, and whiskers extending to the minimum and maximum.

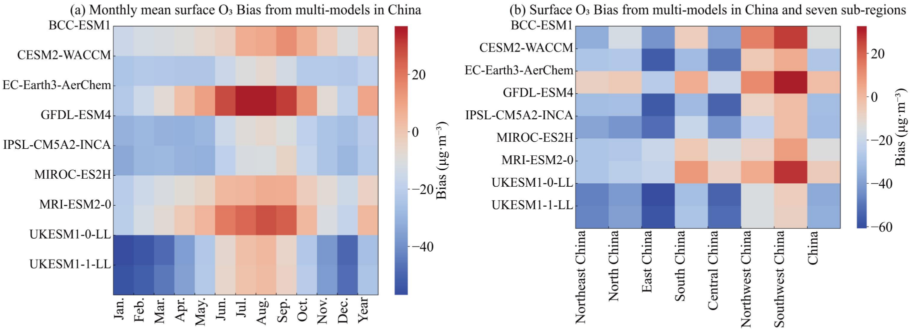

Figure 5. Heatmap of O_3 concentrations Bias from nine CMIP6 models compared to TAP across different months and regions in China and sub-regions.

Figure 4 presents a comparison of the Mean Absolute Error (MAE), Mean Fractional Bias (MFB), and Root Mean Square Error (RMSE) between the CMIP6 models and TAP for surface O_3 concentrations. Combined with the Bias for different months and sub-regions (Figure 5), correlation coefficients, and SD (Figure 6), it can be observed that the MME simulates the O_3 concentration for China with the smallest Bias in June and the largest in January. Among the sub-regions, the simulation results for Northwest China are the most accurate, with high correlation, and the smallest MAE, MFB, RMSE, SD, and Bias. In contrast, the largest MAE, MFB, RMSE, SD, and Bias are found in East China, particularly in the autumn and winter. For individual models, EC-Earth3-AerChem shows the smallest annual average Bias for O_3 concentrations in China, with an MFB close to zero; BCC-ESM1 exhibits the best correlation; MIROC-ES2H has the smallest MAE and RMSE, providing relatively good simulation results; while UKESM1-0-LL has the largest MAE, MFB, RMSE, SD, and Bias. Among the sub-regions, MIROC-ES2H provides relatively good simulations of O_3 concentrations in South China, while UKESM1-0-LL shows the largest MAE, MFB, RMSE, SD, and Bias in East China. Thus,Overall, the MME of CMIP6 performs better in simulating O_3 concentrations during JJA, with larger discrepancies observed in DJF. The simulation in Northwest China is closest to TAP, while the largest discrepancies occur in East China. EC-Earth3-AerChem is better suited for simulating or forecasting the annual average O_3 concentrations over China, while MIROC-ES2H is more appropriate for error-sensitive scenario analyses, BCC-ESM1 demonstrates superior performance in terms of correlation and temporal consistency, whereas both UKESM1-0-LL and UKESM1-1-LL exhibit higher simulation uncertainties.

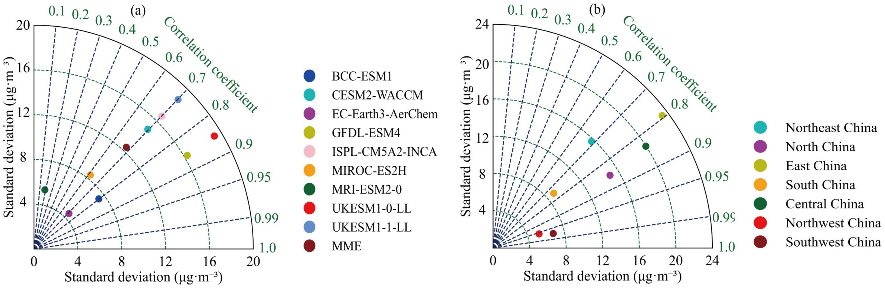

Figure 6. Taylor diagram of the annual mean surface O_3 concentrations simulated by nine CMIP6 models compared with the TAP data during 2014–2023 in China and sub-regions. The radial coordinate shows the standard deviation in the spatial pattern, normalized by the observed standard deviation. The azimuthal variable shows the correlation of the modeled spatial pattern with the observed spatial pattern.

3.2 Under different underlying surface types

Vegetation type, land cover, and land use changes can influence biogenic emissions, which in turn affect the accuracy of model-simulated O_3 concentrations (Ashworth et al., 2012). To investigate the impact of these factors on simulation discrepancies and minimize the interference of temperature changes, this study focuses on the JJA period in Northwest China, which has similar climatic conditions and complex surface types. The selected typical underlying surfaces include natural land surfaces such as grassland, forest, desert, and snow and ice (perennial snow), as well as anthropogenic land surfaces such as cropland and urban. By comparing the Bias, MAE, RMSE, and SD of MME-simulated surface O_3 concentrations relative to TAP (Figure 7), it is observed that TAP simulates lower O_3 concentrations over natural land surfaces compared to anthropogenic land surfaces, and the MME simulations generally follow this trend. However, the MME simulation results show the highest O_3 concentrations over snow and ice surfaces and the lowest over cropland surfaces. Overall, the MME simulations exhibit lower Bias, MAE, and RMSE for natural land surfaces compared to anthropogenic land surfaces, with the best performance over forest and desert surfaces, and the worst performance over urban surfaces, followed by cropland and snow and ice surfaces.

This is likely mainly due to the fact that natural land surfaces have relatively consistent physical and chemical properties, with less human influence, resulting in more accurate O_3 concentration simulations. In contrast, urban surfaces, due to intense human activities and diverse pollution sources (such as transportation and industrial emissions), present a more complex environment, making the

https://doi.org/10.5194/egusphere-2025-4348
Preprint. Discussion started: 25 September 2025

processes of O_3 formation and destruction more intricate and leading to larger discrepancies in the simulation results.

The high albedo of snow and ice surfaces significantly reduces the absorption of solar radiation by the surface, thereby leading to a decrease the intensity of photochemical reactions, particularly the rate of NO_2 photolysis that leads to O_3 formation. In addition, the snow and ice surfaces have a weaker capacity to adsorb O_3, with a deposition velocity ($0.03\ \mathrm{cm \cdot s^{-1}}$) typically lower than other natural land surfaces such as vegetation or soil (Wesely et al., 1981). At the same time, the amount and composition of deposited trace gases, solar irradiance, snow temperature, and the underlying materials beneath the snowpack (e.g., glacier ice, sea ice, frozen soil, and "warm" mid-latitude soils) also affect the process control, intensity, and direction of O_3 flux (Helmig et al., 2007). However, current atmospheric chemistry models may not adequately account for these specificities when simulating O_3 deposition on snow and ice surfaces. For example, deposition rate parameterisation schemes are often based on observations of underlying surface such as vegetation and soil, which do not accurately reflect the physical and chemical properties of snow and ice surfaces. Therefore, compared to other natural land surfaces, the simulation errors in O_3 concentrations over snow and ice surfaces are larger, especially in high-latitude regions or areas with significant snow and ice cover during winter. This also highlights the importance of developing more detailed snow-O_3 exchange parameterizations for improving models.

The simulation bias over cropland may stem from the fact that croplands are often associated with agricultural activities (e.g., fertilization and irrigation), which release large amounts of NO_x and VOCs, thereby increasing the complexity of O_3 formation. Furthermore, changes in vegetation types and management practices in agricultural land can also influence biogenic emissions, further affecting the simulation of O_3 concentrations and leading to larger model biases.

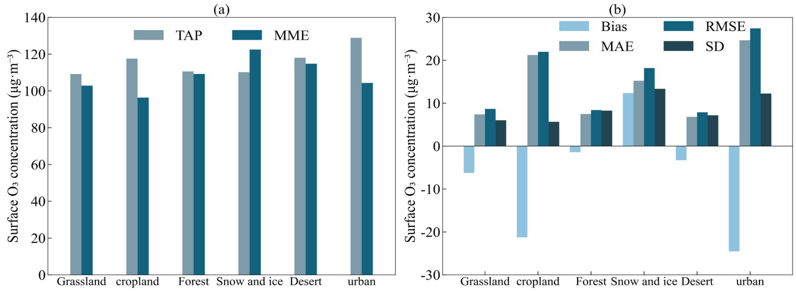

Figure 7. The bias, MAE, RMSE and SD of surface O_3 concentrations simulated by CMIP6 models relative to TAP from 2014 to 2023 over the complex underlying surface in China.

3.3 Under different level of total cloud cover

Referring to the definition of cloud cover levels in weather forecast and the classification of cloud cover level by Han and Cong (2015), the total cloud cover ranging from 0 %–10 % is defined as clear sky, 20 %–30 % as partly cloudy, 40 %–70 % as cloudy, and 80 %–100 % as overcast. This study analyzes the Bias of surface O_3 concentrations simulated by MME relative to those simulated by TAP under different total cloud cover levels (Fig. 8). Analysis results show that the TAP simulation exhibits the highest surface O_3 concentrations under partly cloudy conditions, while under other cloud cover categories, O_3 concentrations generally decrease with increasing total cloud cover (except during JJA). This is primarily attributed to the attenuation of solar radiation by clouds and associated precipitation processes. Clouds reduce incoming solar radiation, thereby slowing photochemical O_3 production. In addition, wet deposition removes certain precursors, further suppressing O_3 formation. Under partly cloudy conditions, however, the atmosphere is generally more stable with weaker vertical mixing, allowing O_3 to accumulate near the surface. However, during JJA, the relationship becomes more complex, high pollutant loads and intricate meteorological conditions likely counteract the influence of total cloud cover, leading to a less straightforward association between cloud amount and O_3 concentrations.

In contrast, the MME simulations do not fully reproduce this pattern. The annual mean bias is smallest under cloudy conditions and largest under partly cloudy conditions. On a seasonal scale, the smallest bias occurs under clear-sky conditions during JJA, while the largest bias is found under partly cloudy conditions. These discrepancies may stem from the complex interactions through which cloud cover influences O_3 by modulating shortwave radiation, photochemical rates, and meteorological variables such as temperature, precipitation, and boundary layer height. They are also closely tied to structural differences among models in physical parameterizations, radiative transfer schemes, and chemical mechanisms.

Therefore, when using CMIP6 models for O_3-related assessment and projection, it is essential to adequately account for the interactions among cloud cover, precipitation, and other key meteorological factors, particularly under polluted and complex meteorological conditions, in order to reduce model uncertainties and improve simulation accuracy (Jacob and Winner, 2009).

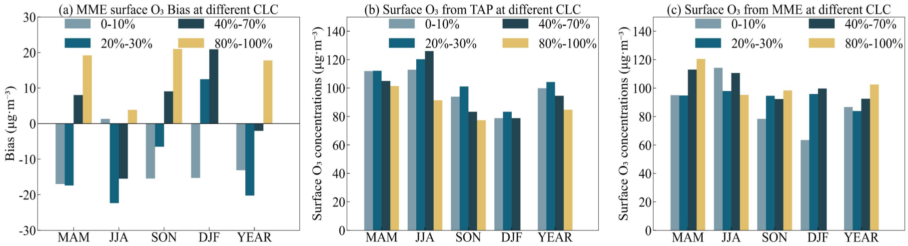

Figure 8. The bias in surface O_3 concentrations simulated by CMIP6 models relative to TAP from 2014 to 2023 under different total cloud cover levels in China.

3.4 Under different concentrations of $PM_{2.5}$ and its components

Aerosols play a crucial role in the simulation of O_3 concentrations, Variations in $PM_{2.5}$ concentrations can influence O_3 concentrations by altering the chemical composition and light absorption characteristics of aerosols, as well as the impact on solar radiation, which in turn affect the rate of photochemical reactions. Lou et al. (2014) used GEOS-Chem simulations to show that the mean Bias in O_3 concentrations for the China is 9% when aerosols are considered, compared to 33% when aerosols are not considered. Therefore, this study analyzes the Bias in surface O_3 concentrations simulated by the MME relative to TAP under different $PM_{2.5}$ levels(Figure 9). The results show that during the JJA and SON, when $PM_{2.5}$ concentrations are relatively low, TAP data indicate an increase in O_3 concentrations with rising $PM_{2.5}$ levels. However, during the DJF, when $PM_{2.5}$ concentrations are higher, O_3 concentrations decrease as $PM_{2.5}$ levels increase. This is primarily due to the fact that, during JJA and SON, although the increase in $PM_{2.5}$ concentrations may have some localized inhibitory effects on O_3 formation, the abundant sunlight and favorable meteorological conditions promote O_3

generation. In contrast, during DJF, due to insufficient sunlight, stronger atmospheric stability, and higher NO_x concentrations, NO_x titration is more likely to occur, which suppresses O_3 formation. At the same time, the increase in BC concentration in $PM_{2.5}$ (Figure S1) enhances the light absorption of $PM_{2.5}$, further reducing UV radiation intensity and thus inhibiting O_3 photochemical production. Additionally, other components of $PM_{2.5}$, such as NO_3 and OM, may also affect O_3 concentrations through various pathways. These factors collectively lead to a decrease in O_3 concentration when $PM_{2.5}$ increases.

The MME simulation results indicate that surface O_3 concentrations generally decrease with increasing $PM_{2.5}$ levels (except during JJA). However, under extreme pollution conditions in DJF, O_3 concentrations exhibit a slight increase once $PM_{2.5}$ exceeds 125 $\mu g \cdot m^{-3}$. This suggests a complex nonlinear relationship between $PM_{2.5}$ and O_3 formation. Previous studies have shown that reducing aerosol emissions without corresponding cuts in precursor pollutants could lead to increased surface O_3 over eastern China (Li et al., 2018), indicating that aerosols suppress O_3 production through light attenuation and heterogeneous reactions. At low to moderate $PM_{2.5}$ concentrations, the increase in $PM_{2.5}$ largely inhibits O_3 formation by scavenging key radicals (e.g., HO_2 and NO_x) and reducing solar radiation intensity, thereby leading to a decline in O_3. However, under extreme pollution conditions, especially in winter, this suppressing effect tends to saturate. Meanwhile, the nocturnal titration of O_3 is weakened under high NO_x conditions, which, combined with unfavorable meteorological conditions such as temperature inversions and a lower boundary layer, results in O_3 concentrations no longer decreasing with further increases in $PM_{2.5}$ and may even slightly increase.

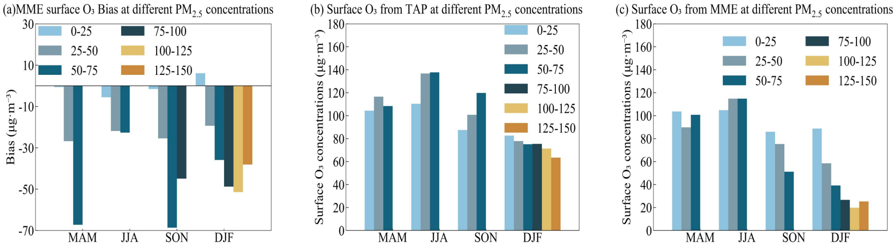

Figure 9. The bias in surface O_3 concentrations simulated by CMIP6 models relative to TAP from 2014 to 2023, under different $PM_{2.5}$ concentrations in China.

These findings highlight that the synergistic and inhibitory effects between $PM_{2.5}$ and O_3 vary significantly across seasons and pollution levels. This implies that future air pollution control strategies should adopt coordinated mitigation of both $PM_{2.5}$ and O_3 precursors to avoid potential side effects from single-pollutant reduction policies.

4 O_3 from the pre-industrial period to present day

This study analyzes the annual mean surface O_3 concentration changes in China and its sub-regions from pre-industrial to present times based on 9 CMIP6 models and MME relative to the 2014–2023 mean (Figure 10). The MME results show that, since 1850, the annual mean surface O_3 concentration in China has increased by $39.3\pm14.4\ \mu g\cdot m^{-3}$ (±1 SD), with the maximum change of $57.9\ \mu g\cdot m^{-3}$ (from the MIROC-ES2H model) and the minimum change of $23.1\ \mu g\cdot m^{-3}$ (from the UKESM1-0-LL model). Before 1950, the annual mean increase in O_3 concentration was relatively slow, at only $0.12\ \mu g\cdot m^{-3}$; however, after 1950, the rate of increase accelerated significantly, with an annual mean increase of $0.28\ \mu g\cdot m^{-3}$. This change is likely primarily related to the significant increase in anthropogenic activities during this period, especially the substantial increase in anthropogenic precursor emissions, such as CH_4, NO_x, CO, and NMVOCs. The simulations of historical O_3 concentrations by different CMIP6 models show that the EC-Earth3-AerChem model yields the highest values, while the IPSL-CM5A2-INCA model yields the lowest. These differences reflect variations in aerosol, climate, and atmospheric chemistry process simulations across different models. Griffiths et al. (2021), based on ground, sounding, and satellite data from the past few decades, assess the performance of multiple CMIP6 models in simulating surface O_3 concentrations. Their study indicates that these models are capable of accurately reproducing the spatial distribution, seasonal variation, and interannual variability and trends of surface O_3 concentrations. This also indicates the reliability of CMIP6 models in simulating historical surface O_3 variations, which provides support for their future projections of O_3 concentrations under climate change scenarios.

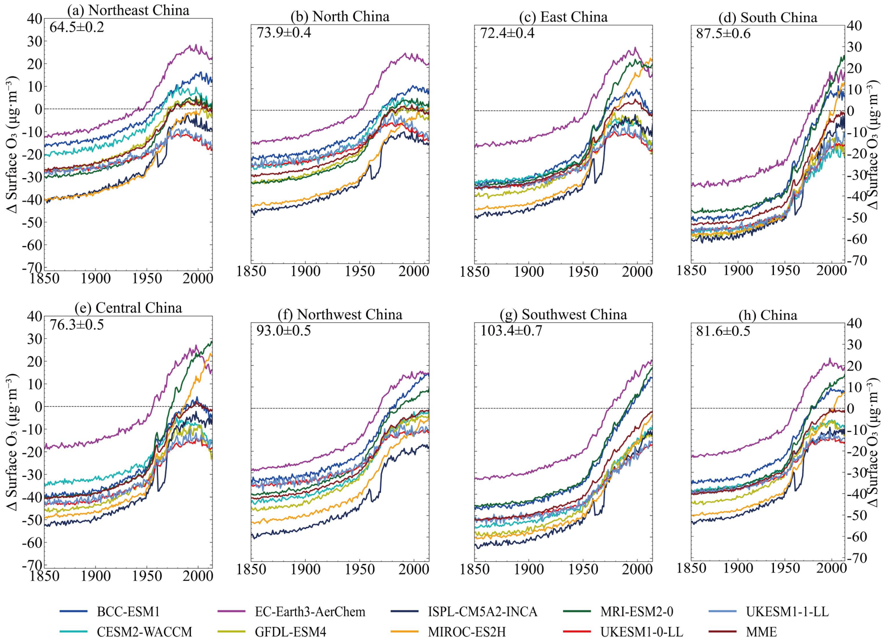

Figure 10. Changes in the China and sub-regions annual mean surface O_3 concentrations from the pre-industrial period to present day, relative to a 2014–2023 mean value, across nine CMIP6 models and MME. The Multi-model annual mean 2014 – 2023 surface O_3 concentrations (±1 SD) are shown in the top left of each panel.

The historical changes in surface O_3 concentrations simulated by different CMIP6 models show significant regional variations, the UKESM1-0-LL model tends to simulate the smallest historical O_3 changes (with the smallest change in Northeast China); while the MIROC-ES2H model simulates the largest O_3 changes (with the largest change in Central China), followed by MRI-ESM2-0 and BCC-ESM1. Although the UKESM1-0-LL simulation has a smallest historical surface O_3 response, it exhibits a larger tropospheric O_3 change during the historical period compared to other CMIP6 models (Griffiths et al., 2021). Moreover, the O_3 change simulated by UKESM1-0-LL is similar to the changes driven solely by precursor emission variations (Turnock et al., 2020), suggesting that this model may be highly sensitive to changes in emission sources when simulating O_3 responses. Central China exhibits the largest discrepancies in historical surface O_3 changes among the CMIP6 models, with the maximum difference reaching 29.6 μg·m^{-3}. Turnock et al. (2020) suggest that the large differences in surface O_3 responses across CMIP6 models can be attributed to variations in the magnitude of simulated O_3 concentrations during the 1850s and the regional average O_3 concentration change rates,

https://doi.org/10.5194/egusphere-2025-4348
Preprint. Discussion started: 25 September 2025

which are closely related to the differing chemical sensitivities of O_3 formation processes to NO_x concentration changes across models. Additionally, the significant changes in $PM_{2.5}$ concentrations in this region (Su et al., 2022) may affect the O_3 formation process by altering the heterogeneous loss rate of aerosols by radicals. Future simulations should further consider the impact of aerosols on O_3 to improve the accuracy of surface O_3 concentration simulations.

5 O_3 from present day to 2100

Figure 11 shows the future changes in surface O_3 concentrations across China and its sub-regions under different CMIP6 scenarios (relative to the 2014–2023 mean). Overall, it is projected that by 2100, surface O_3 concentrations in China will decrease in most scenarios, with sub-regions responding similarly to the national trend, though with varying magnitudes (Figure 12). In the Tier 1 experiment, under the SSP1-2.6 scenario, which involves low radiative forcing, strong climate mitigation, and significant air pollution reduction, surface O_3 concentrations in China are projected to decrease by 12.6±3.1 $\mu g \cdot m^{-3}$ (±1 SD of the MME) by 2050 relative to the 2013–2024 annual mean, and decrease by 25.3±7.2 $\mu g \cdot m^{-3}$ by 2100, with a reduction of approximately 32%. Due to substantial reductions in precursor emissions, a decrease in CH_4 concentrations, and relatively small climate changes, under this scenario, surface O_3 concentrations in all sub-regions also show significant declines. Projections indicate that by 2100, surface O3 concentrations in the Southwest and South China regions will decrease by more than 30 $\mu g \cdot m^{-3}$, while in East China, which experiences the smallest reduction, O_3 concentrations will still decrease by nearly 20 $\mu g \cdot m^{-3}$.

For the medium forcing SSP2-4.5 scenario, it is projected that by 2100, the annual mean surface O_3 concentration in China will decrease by 13.6±7.2 $\mu g \cdot m^{-3}$, with a reduction of 17%. Meanwhile in this scenario, the projections show that the annual mean surface O_3 concentrations in all sub-regions of China will slightly increase in 2055 compared to the 2014–2025 mean, and then start to decrease, by 2100, the reduction will exceed 10 $\mu g \cdot m^{-3}$, with the most significant decrease occurring in South China, where it may reach 24.5 $\mu g \cdot m^{-3}$. This change is primarily driven by enhanced control of precursor emissions, relatively small climate changes, and variations in CH_4 concentrations.

In the SSP3-7.0 scenario, due to weak climate mitigation and weak air pollutant reduction, the annual mean surface O_3 concentration in China is projected to increase by 8.4±2.0 $\mu g \cdot m^{-3}$ by 2050, and increase by 13.9±4.0 μg·m^{-3} by 2100, with an increase of 17%. In this scenario, the annual mean surface O_3 concentrations in all seven sub-regions show an upward trend, with the largest increase in East China, where the concentration is expected to rise by 19.3±6.9 μg·m^{-3} by 2100, with an increase of 27%. Although emissions of O_3 precursors such as NO_x are projected to start decreasing around 2040 (Figure S3), the surface O_3 concentrations in all sub-regions continue to increase, indicating the importance of changes in chemical composition, increasing CH_4 concentrations, and climate change in the simulation of surface O_3 under the SSP3-7.0 scenario (Turnock et al., 2020; Young et al., 2013; Li et al., 2019). Additionally, the projected differences among CMIP6 models are most pronounced in Central and East China, suggesting some divergence in the model simulations of O_3 in these regions.

In the SSP3-7.0-lowNTCF scenario (Tier 2 experiment), strong carbon emission control measures are implemented on top of the weak climate mitigation of the SSP3-7.0 scenario, along with a substantial reduction in short-lived climate forcers (SLCFs), including BC and O_3 precursors, these measures significantly improve air quality and slow down climate change. Consequently, the projections show that under the SSP3-7.0-lowNTCF scenario, the increase in surface O_3 concentrations in China is slower than in the SSP3-7.0 scenario, with relatively lower concentrations. By 2050, the annual mean surface O_3 concentration in China is projected to increase by only 5.8±1.5 μg·m^{-3}, and by 2100, it will increase by 4.9±2.0 μg·m^{-3}, representing a 6% increase. In this scenario, by 2100, surface O_3 concentrations in China and most of its sub-regions are expected to return to or be close to the 2014–2023 levels (especially in the Northwest China), showing a significant improvement in surface O_3 pollution compared to the SSP3-7.0 scenario. However, compared to other regions of the world, the additional reduction in precursor emissions under the SSP3-7.0-lowNTCF scenario has a relatively small impact on improving surface O_3 pollution in China. This is mainly due to the increase in surface O_3 concentrations in eastern China (especially in Central and Eastern China). This increase is caused by a slight rise in NMVOCs emissions and a reduction in O_3 titration due to a significant decrease in NO_x emissions (Turnock et al., 2020). Additionally, the decrease in $PM_{2.5}$ concentrations under the SSP3-7.0-lowNTCF scenario leads to a reduction in the heterogeneous loss of free radicals, which may also contribute to the rise in surface O_3 concentrations (Li et al., 2019).

In the SSP5-8.5 scenario, characterized by high radiative forcing, weak climate mitigation, and weak air pollutant emission reductions, the annual mean surface O_3 concentration in China is projected to increase by 6.3±1.6 μg·m^{-3} by 2050. However, by 2100, the surface O_3 concentration is expected to decrease by 3.4±2.9 μg·m^{-3} relative to the 2013–2024 mean, a reduction of approximately 4.2%. The projected changes in surface O_3 concentrations for the sub-regions in this scenario are similar to those in the SSP3-7.0-lowNTCF scenario (with a correlation of up to 0.7), likely due to comparable levels of air pollutant emissions and climate change. By 2050, the surface O_3 concentration in most sub-regions will increase slightly faster in the SSP5-8.5 scenario than in the SSP3-7.0-lowNTCF scenario (except for Northeast and North China), but slower than in the SSP3-7.0 scenario (except for Central and East China). This may be attributed to the different changes in CH_4 emissions under different scenarios. Additionally, more CMIP6 model data are available for the SSP3-7.0 scenario (9 models) compared to the SSP5-8.5 scenario (4 models), which may also influence the MME response.

In the Tier 2 experiment, under the SSP1-1.9 scenario, the annual mean surface O_3 concentration in China is projected to decrease by 16.6±7.1 μg·m^{-3} by 2050, and decrease by 25.3±9.5 μg·m^{-3} by 2100, with a reduction of approximately 32%. Although the SSP1-1.9 scenario represents weak climate mitigation and weak air pollutant emission reductions, the simulated results indicate a significant decrease in surface O_3 concentrations. This phenomenon may be closely related to the reduction of $PM_{2.5}$ emissions in China and the complex effects of climate change. Specifically, climate change not only alters the rates of chemical reactions in the atmosphere but also impacts convection activities and the distribution of pollutants, thereby inhibiting O_3 formation or altering the balance between its formation and consumption. Furthermore, the reduction of $PM_{2.5}$ may further exacerbate the decline in surface O_3 concentrations by influencing atmospheric photochemical processes or altering the concentrations of O_3 precursors.

Under the SSP4-3.4 and SSP4-6.0 scenarios, which represent moderate climate mitigation with moderate air pollutant emission reductions, and under the SSP5-3.4-over scenarios which represents moderate climate mitigation with stronger air pollutant emission reductions, the surface O_3 concentration in China is projected to increase by 13.5±1.3 μg·m^{-3}, 18.3±1.4 μg·m^{-3}, and 12.6±1.6 μg·m^{-3} by 2050, respectively. By 2100, the surface O_3 concentrations are expected to decrease by 9.2±8.3 μg·m^{-3}, 1.6±5.9 μg·m^{-3}, and 13.9±11.7 μg·m^{-3} respectively. This trend indicates that strong air pollutant emission reduction measures will play a significant role in controlling future O_3 concentrations, improving air quality and mitigating negative climate impacts.

In summary, projections from the CMIP6 models suggest that mitigating surface O_3 pollution across China will require not only reducing greenhouse gas emissions to moderate future climate change but

https://doi.org/10.5194/egusphere-2025-4348
Preprint. Discussion started: 25 September 2025

also implementing enhanced controls on emissions of O_3 precursors (including CH_4). Under scenarios with pronounced climate change impacts, such as SSP3-7.0 and SSP5-8.5, the stringency of controls on 560 key O_3 precursors, particularly NMVOCs and NO_x, beyond 2050 is expected to lead to divergent regional responses in long-term surface O_3 trends.

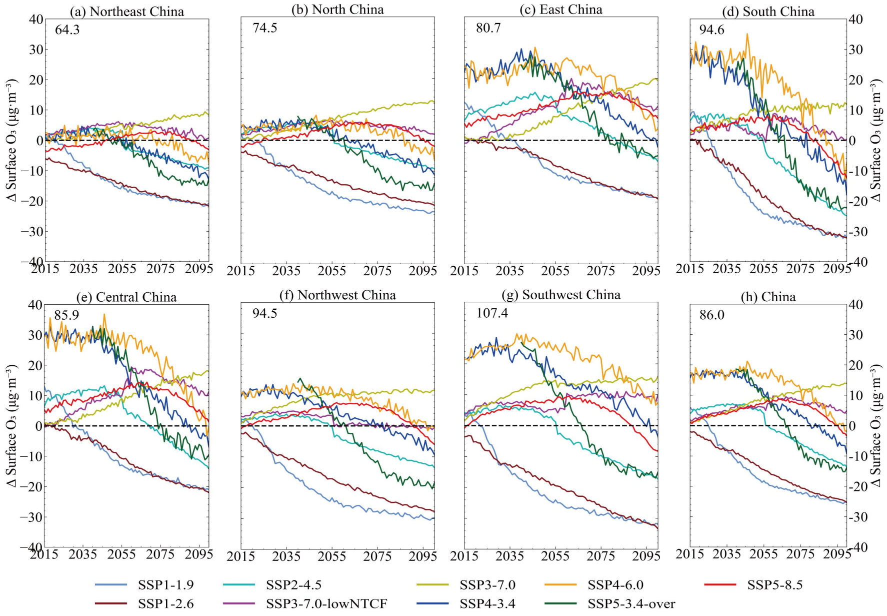

Figure 11. Future China and sub-regions changes in annual mean surface O_3 for the different SSPs used in 565 CMIP6. The dashed black line represents the curve of the difference at zero. The multi-model regional mean value for the years 2014–2023 mean value is shown in the top left corner of each panel.

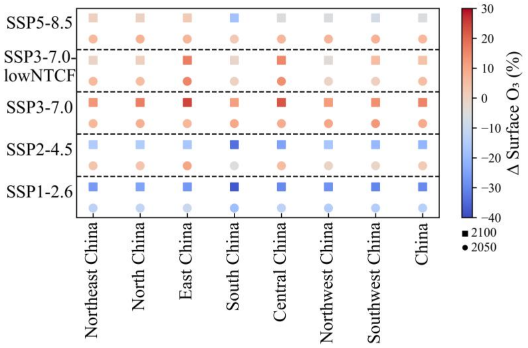

Figure 12. Percentage change in 2050 (circles) and 2100 (squares), relative to 2015, for annual mean of O_3 570 across China and sub-regions in the four Tier 1 future CMIP6 scenarios and the SSP3-7.0-lowNTCF scenario.

Since the number of available CMIP6 models is the greatest under the SSP3-7.0 scenario (Table 1), this paper conducts a comparative analysis of the changes in surface O_3 concentrations across China and its sub-regions under the SSP3-7.0 scenario, aiming to identify the potential causes of model discrepancies. Figure 13 illustrates the changes in the annual mean and seasonal mean surface O_3 concentrations in China and its sub-regions for the years 2050 (2045–2055 mean) and 2095 (2090–2100 mean) relative to the 2014–2023 mean baseline, based on different CMIP6 models under the SSP3-7.0 scenario. O_3 is not directly emitted into the troposphere but is produced through photochemical oxidation of CO, CH_4, and NMVOCs in the presence of NO and NO_2. The abundance of tropospheric O_3 is determined by its budget, which includes chemical production, stratospheric transport, chemical loss, and deposition to the surface (Lelieveld and Dentener, 2000), and the intensity of these processes is highly sensitive to current climate conditions and the emissions and distribution of O_3 precursors (including NO_x, NMVOCs, CH4, etc.). Therefore, this study further analyzes the correlation between future annual mean surface O_3 concentrations under the SSP3-7.0 scenario and other variables, including CH_4 concentrations, Near-Surface Air Temperature (TAS), NO_x concentrations, total emissions of NMVOCs and BVOCs (Figure 14).

It can be observed that surface O_3 concentrations predicted by different CMIP6 models under the SSP3-7.0 scenario exhibit significant regional discrepancies. In particular, in Central China, the O_3 concentrations predicted by MRI-ESM2-0 and EC-Earth3-AerChem are nearly twice as high as those predicted by UKESM1-0-LL and GFDL-ESM4 (Figure S2). The lower annual mean O_3 concentrations in Central China for UKESM1-0-LL and GFDL-ESM4 are primarily attributed to higher NO_x emissions under the SSP3-7.0 scenario. In this region, NO_x emissions are approximately 2–3 times higher than those in the other two models (Figure S2), which likely triggers NO_x titration and results in lower simulated surface O_3 concentrations. In contrast, in the MRI-ESM2-0 and EC-Earth3-AerChem, NO_x titration is rare during DJF, and the CH_4 concentration is higher in the EC-Earth3-AerChem model (Fig. S4), resulting in higher simulated O_3 concentrations in Central China. These discrepancies highlight that, although the driving factors related to O_3 changes (such as climate change and pollutant emissions) are crucial in all models (Figure 14), the differences in precursor emissions (NO_x and CH_4) and chemical process responses between models in future scenarios with significant climate change have a substantial impact on regional O_3 concentration predictions.

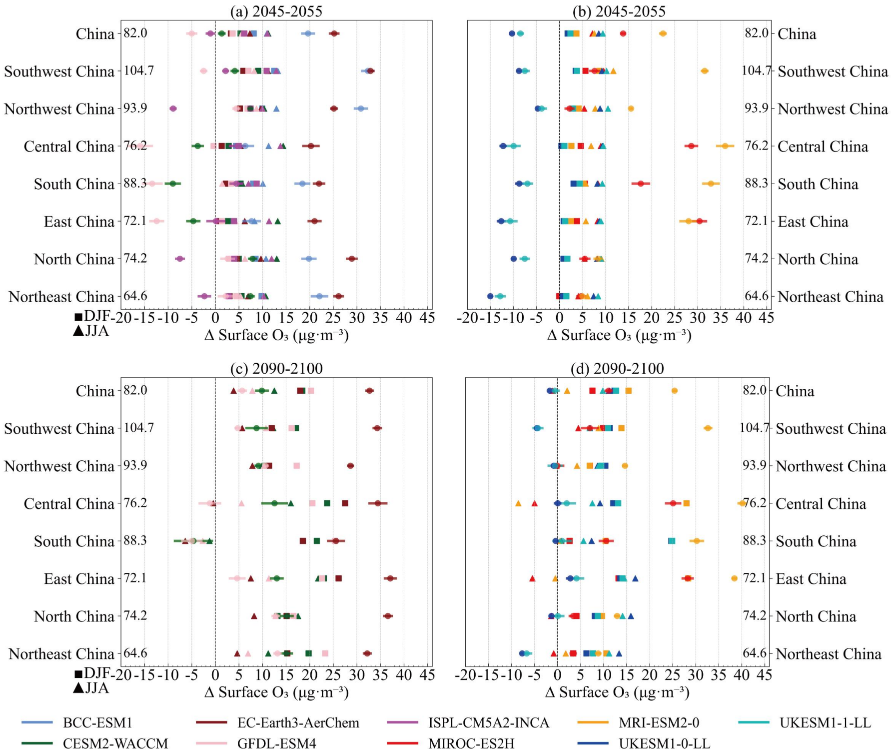

Figure 13. Changes in the annual and seasonal mean surface O_3 in China and its sub-regions, relative to the 2014–2023 mean, for the SSP3-7.0 scenario used in CMIP6. Each coloured circle represents the annual mean response for an individual model in (a) and (b) for 2045–2055, and in (c) and (d) for 2090–2100, with the coloured bars showing the SD across the annual mean. The seasonal mean responses for DJF and JJA, averaged over the relevant 10-year periods, are shown by squares and triangles, respectively. The Multi-model regional mean for the 2014–2023 period is shown on the left of each panel.

IPSL-CM5A2-INCA (predictions extending only to 2055) under the370 scenario, which projects that by 2050, surface O_3 concentrations in northern China (including Northeast, North, and Northwest China) will be lower than the 2014–2023 mean, with the most significant decrease expected in North China, where O_3 concentrations are projected to drop by approximately 10%. IPSL-CM5A2-INCA (ECS; 3.6 K) is a model with moderate equilibrium climate sensitivity, showing a moderate response to global temperature increases caused by greenhouse gases. The model simulates relatively high BVOCs emissions during the 2014–2023 period (covering a broader range of BVOCs types), with emissions approximately 4–8 times higher than those of other models (Figure S5), and these emissions have shown a consistent upward trend. However, despite the increase in BVOCs emissions, this model

https://doi.org/10.5194/egusphere-2025-4348
Preprint. Discussion started: 25 September 2025

simulates relatively low NO_x concentrations and surface TAS, resulting in a smaller increase in O_3 concentrations, and even a decrease in some regions. This indicates that differences in the magnitude of climate change and O_3 precursor (NO_x) variations, as well as the different ways these factors are coupled in different CMIP6 models, lead to significant differences in the response of the models to BVOCs emissions. Such differences could directly influence future surface O_3 changes, particularly in localized regions.

CESM2-WACCM and GFDL-ESM4 under the SSP3-7.0 scenario, on the other hand, predict that by 2050, surface O_3 concentrations in southern China (including East, Central, and South China) will be lower than the 2014–2023 annual mean, with the most significant decrease observed in South China, where O_3 concentrations are projected to drop by 9% and 13% in the two models, respectively. Firstly, CESM2-WACCM (ECS; 4.7 K) and GFDL-ESM4 (ECS; 4.4 K) exhibit higher climate sensitivity, meaning that their projected temperature increase and water vapor increase are more significant. Higher temperatures and water vapor content facilitate the generation of OH radicals, which in turn accelerate O_3 destruction reactions (Wild et al., 2020). In tropical and subtropical regions, where both temperature and water vapor are already high, the presence of these factors may further enhance the consumption of O_3 by OH radicals, a phenomenon particularly evident in South China. Secondly, both models tend to simulate lower BVOCs emissions (Figure S5), with GFDL-ESM4 showing the lowest and virtually unchanged BVOCs emissions under the SSP3-7.0 scenario, which may reduce the formation of O_3. Furthermore, the pollutant emissions and atmospheric chemical processes in southern China differ from those in the north. The southern regions are likely more dependent on photochemical reactions, which are more active under higher temperatures and stronger solar radiation conditions. Therefore, CESM2-WACCM and GFDL-ESM4 may simulate a greater number of photochemical reactions, further accelerating O_3 decomposition.

Under the SSP3-7.0 scenario, both UKESM1-0-LL and UKESM1-1-LL project that surface O_3 concentrations across China and its sub-regions will decrease by 2050 relative to the 2014–2023 annual mean, with the most significant decrease observed in Northeast China, where the reduction is projected to be 23% and 20% for the two models, respectively. Although a moderate increase is projected by 2095, O_3 concentrations remain below the 2014–2023 baseline in most regions, except East China. Compared to other CMIP6 models, UKESM1-0-LL (ECS; 5.4 K) and UKESM1-1-LL (ECS; 4.2 K) exhibit higher climate sensitivities. The elevated temperatures (Figure S7) and altered climatic conditions in these models likely enhance O_3 degradation, contributing to the generally lower O_3 concentrations in their simulations. Moreover, UKESM1-0-LL simulates higher atmospheric NO_x levels, promoting NO_x titration that suppresses O_3 formation. This model also projects higher NMVOCs emissions (Figure S6). Under high-NO_x conditions, the interplay between NO_x and NMVOCs can modify photochemical O_3 production pathways, further inhibiting net O_3 formation (Jiménez & Baldasano; Xing et al., 2011). To further investigate this mechanism, we constructed a two-dimensional framework based on ground observations, analyzing O_3 distribution across China within the NO_2-NMVOCs space (Figure 15). Results indicate that the highest O_3 levels occur under moderate NO_2 (20–40 $\mu g \cdot m^{-3}$) and elevated NMVOCs (>500 $t \cdot month^{-1}$) conditions, reflecting a typical VOC-limited O_3 formation regime. In such environments, abundant NMVOCs coupled with relatively low NO_x levels promote efficient photochemical O_3 production. However, when NO_2 concentrations reach 60–120 $\mu g \cdot m^{-3}$, O_3 decreases significantly even at intermediate-to-high NMVOCs, indicating strong inhibition of O_3 formation by excess NO_x.

The projections of annual mean surface O_3 concentrations for China and its sub-regions under the SSP3-7.0 scenario by BCC-ESM1 (ECS; 4.0K, predictions extending only to 2055), EC-Earth3-AerChem (ECS; 3.0K), MIROC-ES2H (ECS; 3.6K), and MRI-ESM2-0 (ECS; 5.4K) show significant consistency, with O_3 concentrations in 2050 and 2095 both being higher than the 2014–2023 mean. Among these models, MIROC-ES2H and MRI-ESM2-0 exhibit higher climate sensitivity, although their projected NO_x and CH_4 concentrations are relatively low (Figure S3–S4), they still tend to predict larger increases in O_3 compared to the other models, with the most significant O_3 increase observed in southern China (including East China, Central China, and South China). In contrast, BCC-ESM1 and EC-Earth3-AerChem predict more noticeable increases in O_3 concentrations in northern China (including Northeast, North, Northwest, and Southwest China). EC-Earth3-AerChem, with a relatively low ECS, simulates lower NO_x concentrations in China and its sub-regions, while its CH_4 concentrations are the highest among the models (Figure S4). Under low NO_x conditions and a weak NO_x titration effect, an increase in CH_4 promotes O_3 formation, leading to O_3 accumulation and a more pronounced increase in simulated O_3 concentrations in the model. BCC-ESM1, on the other hand, tends to simulate higher NO_x concentrations and lower TAS (Figure S3 and S7), which contributes to the more noticeable O_3 increase predicted by this model.

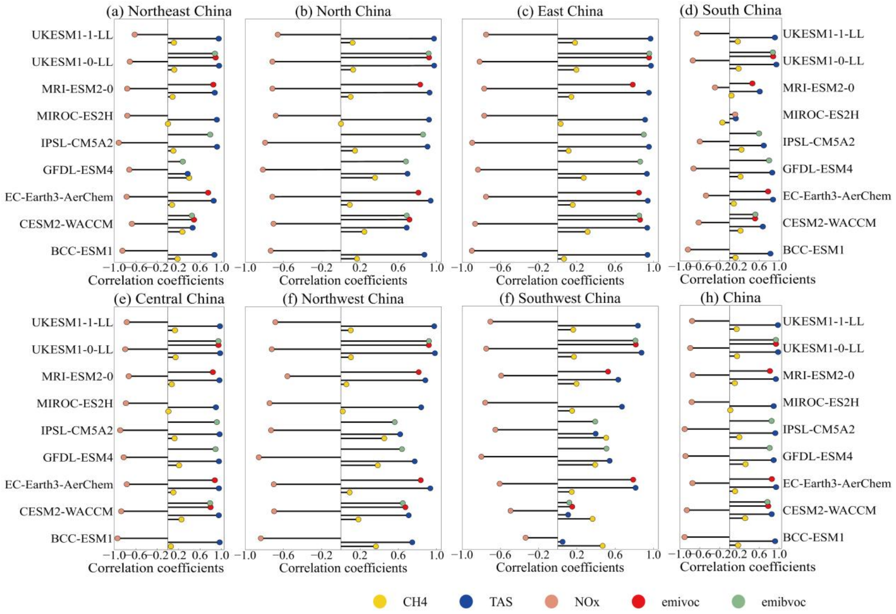

Figure 14. Correlation coefficients calculated when comparing future annual mean surface O_3 concentrations against individual variables of surface CH_4 concentrations, temperature at Surface (TAS), emissions of NMVOCs and BVOCs, NO_x ($NO + NO_2$) concentrations and from individual CMIP6 models over the period 2015 to 2100 in the SSP3-7.0 scenario.

The seasonal responses of different models under the SSP3-7.0 scenario also show variations across sub-regions. Most models predict that surface O_3 concentrations increase more in JJA than in DJF. However, some regions exhibit a decreasing trend in O_3 concentrations during JJA, which aligns with the findings of Turnock et al. (2020).

As shown in Figure 14, under the SSP3-7.0 scenario, a negative correlation between surface O_3 and NO_x concentrations is observed across China and its sub-regions in all the CMIP6 models compared, which may be related to the higher NO_x emissions in the region, leading to the occurrence of NO_x titration. In this scenario, NO_x reacts with surface O_3, depleting a significant amount of O_3. As NO_x emissions decrease under this scenario (after 2030), the NO_x titration effect weakens, thereby promoting O_3 formation at the surface. Consequently, under the SSP3-7.0 scenario, as NO_x emissions decrease, surface O_3 concentrations in China and its sub-regions show an increasing trend. Furthermore, most CMIP6 models exhibit positive correlations between other variables (TAS, CH_4, NMVOCs, and

BVOCs), indicating that climate change and anthropogenic activities are also important drivers of the increase in surface O_3 concentrations in the region.

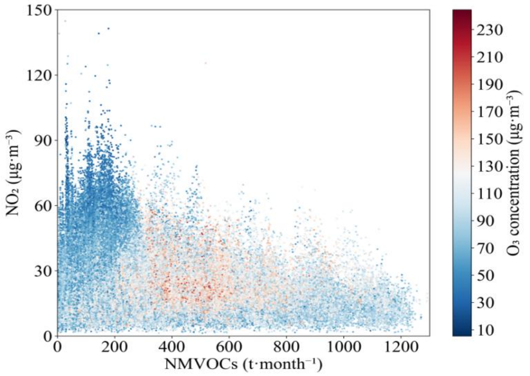

Fig. 15 Distribution of O_3 concentration in NO_2-NMVOCs coordinate in China

The differences in simulations between different CMIP6 models highlight the importance of further understanding how future O_3 concentrations will be influenced by the combined effects of pollutant emissions (especially with regard to the differences in how O_3 precursors, $PM_{2.5}$, and other factors are coupled and how chemical processes respond across models) and climate change. For example, in the Central China region, the prediction differences between models are highly significant, with some models predicting O3 concentrations that could be twice as high as those of others. This discrepancy reflects the need for future research to focus more on model uncertainty in order to improve the accuracy of future air quality predictions.

6 Summary

In recent years, with the increase in industrial activities and transportation, O_3 concentrations in the atmosphere have risen significantly, leading to profound impacts on the global climate system and human health. Therefore, an in-depth study of O_3 changes over historical periods and under different future scenarios, as well as its interactions with climate mitigation measures, is essential for assessing the potential impacts of O_3 on the climate and human health. CMIP6 provides a valuable opportunity to evaluate the simulations of historical and future air pollutant changes using the latest generation of earth system and climate models, based on the most recent socio-economic development scenarios.

https://doi.org/10.5194/egusphere-2025-4348
Preprint. Discussion started: 25 September 2025

This study, based on the CMIP6 multi-model O_3 products and the TAP dataset, analyzes the surface O_3 distribution in China and its sub-regions by nine CMIP6 models, as well as the reasons for the uncertainties in these simulations. It also presents the historical changes of surface O_3 in China and its sub-regions from 1850 to 2014, and evaluates the future changes in surface O_3 under different scenarios (from weak to strong air pollutants and climate mitigation) simulated by the CMIP6 models for China and its sub-regions. The main conclusions are as follows:

(1) The MME of CMIP6 simulated O_3 concentrations in China are higher in JJA, with an average value of 105 $\mu g \cdot m^{-3}$, and lowest in DJF, with a value of 55 $\mu g \cdot m^{-3}$.Among the seven sub-regions, the highest O_3 concentrations in JJA are found in Central China, while in the other three seasons, the Southwest region has noticeably higher O_3 concentrations compared to other regions, especially in Tibet. Nine CMIP6 models show significant underestimation in most regions of China, with the most pronounced underestimation occurring in East China, where the difference is greatest. The Southwest China is slightly overestimated, while the simulated values for the Northwest China are closest to the TAP data. All CMIP6 models perform better in JJA simulations, while the differences are larger in DJF. Among these, EC-Earth3-AerChem, MIROC-ES2H, and BCC-ESM1 produce better simulations, while UKESM1-0-LL and UKESM1-1-LL show larger discrepancies, with more severe underestimation.

(2) The Bias, MAE, and RMSE of O_3 concentrations simulated by MME on natural land surfaces are all lower than those on anthropogenic land surfaces. Among these, the simulation performs best on forest and desert surfaces, while its performance is relatively poorer on urban surface. The Bias of annual mean surface O_3 simulated by MME is lowest under cloudy conditions and highest under partly cloudy conditions, while for seasonal averages, the variability is smallest under clear-sky conditions in the summer and largest under less cloudy conditions in the summer. The MME simulations generally show a decrease in surface O_3 concentrations with increasing $PM_{2.5}$ levels (except in JJA), however, during the DJF, when $PM_{2.5}$ concentrations are high, O_3 concentrations increase instead when $PM_{2.5}$ concentrations exceed a certain threshold. Furthermore, The Bias of O_3 concentrations simulated by MME generally increases with the increase in $PM_{2.5}$ concentrations, but once the $PM_{2.5}$ concentrations exceed a certain threshold value, the Bias then begins to decrease. This also indicates that the effects of meteorological conditions, subsurface type, cloud cover, pollutant concentration, etc. need to be further considered when modelling O_3 concentration.

(3) Over the entire historical period (1850–2014), the MME-simulated an increase of 39.3 μg·m^{-3} in the annual mean surface O_3 concentration in China, with the maximum change of 57.9 μg·m^{-3} (from the MIROC-ES2H model) and the minimum change of 23.1 μg·m^{-3} (from the UKESM1-0-LL model). Before 1950, the annual mean increase in O_3 concentration was relatively slow, at only 0.12 μg·m^{-3}; however, after 1950, the rate of increase accelerated significantly, with an annual mean increase of 0.28 μg·m^{-3}. There are significant discrepancies in the historical changes simulated by different models across various sub-regions, with UKESM1-0-LL tending to simulate the smallest historical changes (smallest in Northeast China), and MIROC-ES2H simulating the largest changes (largest in Central China). Central China is also the region with the greatest diversity of simulated historical changes in surface O_3, with a maximum difference of up to 29.6 μg·m^{-3} among multi-model simulations.

(4) Under the weak mitigation scenarios (SSP3-7.0 and SSP5-8.5), the MME projects an increase in surface O_3 concentrations across most sub-regions of China under SSP3-7.0,driven by the combined effects of increased air pollutant emissions, higher global CH_4 abundance, and climate change. This increase is particularly pronounced in East China, where surface O_3 is projected to rise by 19.3 μg·m^{-3} by 2100, a 26.9% increase. Under SSP5-8.5, surface O_3 is expected to increase by 2050, but decrease by 2100, especially in South China with a decrease of 12.5 μg·m^{-3} by 2100, a decrease of 14.6%. The SSP3-7.0-lowNTCF predicts relatively small changes in surface O_3 across China, with a slight increase (a 4.9 μg·m^{-3} rise by 2100, a 6% increase). In contrast, under the strong climate mitigation and significant air pollutant emission reduction scenario (SSP1-2.6), surface O_3 concentrations are projected to decrease across China, particularly in Southwest and South China, where reductions exceed 30 μg·m^{-3}. In medium climate mitigation scenarios (SSP2-4.5, SSP4-3.4, SSP4-6.0, and SSP5-3.4-over), surface O_3 is expected to increase by 2050, but decrease by 2100. Although SSP1-1.9 represents a weak climate mitigation and weak air pollution reduction scenario, its simulated results show a significant decrease in surface O_3, which may be closely related to the reduction of $PM_{2.5}$ in China and the complex effects of climate change.

(5) The projected surface O_3 concentrations over China and its sub-regions vary significantly among different climate models, reflecting discrepancies in how these models handle climatic factors (e.g., TAS), atmospheric circulation processes, key chemical reactions (involving NO_x and CH_4), and precursor emissions (such as NMVOCs and BVOCs), these differences contribute to substantial uncertainties in regional O_3 simulations, particularly in Central China. Under the SSP3-7.0 scenario,

there is a negative correlation between surface O_3 and NO_x concentrations, likely due to the occurrence of the NO_x titration effect. In addition, surface O3 shows a positive correlation with other variables (TAS, CH4, NMVOCs, and BVOCs) in most CMIP6 models, indicating that climate change and human activities are also important drivers of surface O_3 increases in this region.

This study analyzes the simulation of surface O_3 distributions and the reasons for their biases by different CMIP6 models under various conditions, including different temperatures, cloud cover, complex underlying surface, and pollutant concentrations in China and its sub-regions. For the SSP3-7.0, this paper also discusses the interactions between surface O_3 concentrations and chemical species (NO_x and CH_4), climate factors (TAS), and natural precursor emissions (NMVOCs, BVOCs), and analyzes the reasons behind the differences in O_3 simulations among the CMIP6 models. It is noteworthy that, although the driving factors related to O_3 changes are important across all models, significant differences exist in the coupling methods and chemical process responses of the models in regions with large changes in pollutant emissions (such as O_3 precursors, $PM_{2.5}$, etc.) under future scenarios with significant climate change. A deeper understanding of the mechanisms behind these differences is crucial for comprehending future O_3 trends, developing effective air quality management strategies, and improving the ability to predict future regional air quality. Additionally, the ground-based observation data used in this study are relatively limited, and future research should incorporate more satellite observation data with high spatial and temporal resolution to enrich related studies and discussions.

Data availability. The CMIP6 data can be accessed and downloaded at https://aims2.llnl.gov/search/cmip6/ (last access: 8 September 2024). TAP data can be and downloaded at http://tapdata.org.cn/ (last access: 22 July 2024).

Author contributions. Shuai Li, Hua Zhang, Qi Chen, Yonghang Chen, Zhili Wang, Qi An and Xinping Wu designed the study. Xinping Wu and Qi An carried out the data collection. Shuai Li, Qi Chen and Yonghang Chen carried out the data processing and analysis. Shuai Li, Hua Zhang, and Zhili Wang assisted with the interpretation of results. All co-authors contributed to writing and reviewing the paper.

Competing interests. The authors declare that they have no conflict of interest.

Acknowledgements. We are grateful to the the Earth System Grid Federationr for CMIP6 data support. We further acknowledge the Tsinghua University for TAP data support. We thank the editors and anonymous reviewers, whose comments and suggestions improved the utility and readability of this paper.

Financial support. This work was financially supported by the National Key R&D Program of China (grant no. 2022YFC3701202&2017YFA0603502), the National Natural Science Foundation of China (grant no. 42275039), and the S&T Development Fund of CA MS (fund no. 2024KJ021).

References

An, Q. , Zhang, H., Zhao, S. ,Wang, T., Liu, Q., Wang, Z., Gong, S., Xie, B., and Liu, Y.: Updated Simulation of Tropospheric Ozone and Its Radiative Forcing over the Globe and China Based on a Newly Developed Chemistry-Climate Model, J. Meteor. Res., 36(4), 553–573, https://doi.org/10.1007/s13351-022-1187-2, 2022.

Ashworth, K., Folberth, G., Hewitt, C. N., and Wild, O.: Impacts of near-future cultivation of biofuel feedstocks on atmospheric composition and local air quality, Atmos. Chem. Phys., 12, 919–939, https://doi.org/10.5194/acp-12-919-2012, 2012.

Avnery, S., Mauzerall, D. L., Liu, J., and Horowitz, L. W.: Global crop yield reductions due to surface ozone exposure: 1. Year 2000 crop production losses and economic damage, Atmos Environ., 45: (13), 2284–2296, https://doi.org/10.1016/j.atmosenv.2010.11.045, 2011.

Coates, J., Mar, K. A., Ojha, N., and Butler, T. M.: The influence of temperature on ozone production under varying NO_x conditions - a modelling study, Atmos. Chem. Phys., 16(18), 11601–11615, https://doi.org/10.5194/acp-16-11601-2016, 2016.

Collins, W. J., Lamarque, J. F., Schulz, M., Boucher, O., Eyring, V., Hegglin, M. I., aycock, A., Myhre, G., Prather, M., Shindell, D., and Smith, S.J.: AerChemMIP: quantifying the effects of chemistry and aerosols in CMIP6, Geosci. Model Dev., 10, 585–607, https://doi.org/10.5194/gmd-10-585-2017, 2017.

Dai, H. B., Zhu, J., Liao, H., Li, J. D., Liang, M. X., Yang, Y., and Yue, X.: Co-occurrence of ozone and $PM_{2.5}$ pollution in the Yangtze River Delta over 2013–2019: spatiotemporal distribution and meteorological conditions, Atmos. Res., 249, 105363, https://doi.org/10.1016/j.atmosres.2020.105363, 2020.

Emmons, L. K., Schwantes, R. H., Orlando, J. J., Tyndall, G., Kinnison, D., Lamarque, J., Marsh, D., Mills, M. J., Tilmes, S., Bardeen, C., Buchholz, R. R., Conley, A., Gettelman, A., Garcia, R., Simpson, I., Blake, D. R., Meinardi, S., and Pétron, G.: The Chemistry Mechanism in the Community Earth System Model Version 2 (CESM2), J. Adv. Model. Earth Syst., 12, 1–21, https://doi.org/10.1029/2019ms001882, 2020.

Eyring, V., Bony, S., Meehl, G. A., Senior, C. A., Stevens, B., Stouffer, R. J., and Taylor, K. E.: Overview of the Coupled Model Intercomparison Project Phase 6 (CMIP6) experimental design and organization, Geosci Model Dev., 9, 1937–1958, https://doi.org/10.5194/gmd-9-1937-2016, 2016.

Feng, Z. Z., Calatayud V., Zhu J. G., and Kobayashi, K.: Ozone exposure-and flux-based response relationships with photosynthesis of winter wheat under fully open air condition, Sci. Total Environ., 619/620, 1538-1544, https://doi.org/10.1016/j.scitotenv.2017.10.089, 2018.

Griffiths, P. T., Murray, L. T., Zeng, G., Shin, Y. M., Abraham, N. L., Archibald, A. T., Deushi, M., Emmons, L. K., Galbally, I. E., Hassler, B., Horowitz, L. W., Keeble, J., Liu, J., Moeini, O., Naik, V., O'Connor, F. M., Oshima, N., Tarasick, D., Tilmes, S., Turnock, S. T., Wild, O., Young, P. J., and Zanis, P.: Tropospheric ozone in CMIP6 Simulations, Atmos. Chem. Phys., 21, 4187–4218, https://doi.org/10.5194/acp-21-4187-2021, 2021.

Haase, S. and Matthes, K.: The importance of interactive chemistry for stratosphere-troposphere coupling, Atmos. Chem. Phys., 19(5), 3417–3432, https://doi.org/10.5194/acp-19-3417-2019, 2019.

Hajima, T., Watanabe, M., Yamamoto, A., Tatebe, H., Noguchi, M. A., Abe, M., Ohgaito, R., Ito, A., Yamazaki, D., Okajima, H., Ito, A., Takata, K., Ogochi, K., Watanabe, S., and Kawamiya, M.: Development of the MIROC-ES2L Earth system model and the evaluation of biogeochemical processes and feedbacks, Geosci. Model Dev., 13, 2197–2244, https://doi.org/10.5194/gmd-13-2197-2020, 2020.

Han, Y. Q., and Cong, C. H.: Analysis and validation of FY-2E total cloud amount productions in north China and Huanghuai area, J. Meteor. Environ., 31(5), 153–158, http://www.jme1984.net.cn/CN/Y2015/V31/I5/153 (last access: 1 December 2024), 2015 (in Chinese with English abstract).

Helmig, D., Ganzeveld, L. N. , Butler, T., and Oltmans, S. J.: The role of ozone atmosphere-snow gas exchange on polar, boundary-layer tropospheric ozone – a review and sensitivity analysis, Atmos. Chem. Phys., 7, 15–30, https://doi.org/10.5194/acp-7-15-2007, 2007.

Horowitz, L. W., Naik, V., Paulot, F., Ginoux, P. A., Dunne, J. P., Mao, J., Schnell, J., Chen, X., He, J., John, J. G., Lin, M., Lin, P., Malyshev, S., Paynter, D., Shevliakova, E., and Zhao, M.: The GFDL Global Atmospheric ChemistryClimate Model AM4.1: Model Description and Simulation Characteristics, J. Adv. Model. Earth Syst., 12, e2019MS002032, https://doi.org/10.1029/2019MS002032, 2020.

Hubert, D., Heue, K. P., Lambert, J. C., Verhoelst, T., Allaart, M., Compernolle, S., Cullis, P. D., Dehn, A., Félix, C., Johnson, B. J., Keppens, A., Kollonige, D. E., Lerot, C., Loyola, D., Maata, M., Mitro, S., Mohamad, M., Piters, A., Romahn, F., Selkirk, H. B., da Silva, F. R., Stauffer, R. M., Thompson, A. M., Veefkind, J. P., Vömel, H., Witte, J. C., and Zehner, C.: TROPOMI tropospheric ozone column data: geophysical assessment and comparison to ozonesondes, GOME-2B and OMI, Atmos. Meas. Tech., 14, 7405–7433, https://doi.org/10.5194/amt-14-7405-2021, 2021.

Ivanciu, I., Matthes, K., Wahl, S., Harlaß, J., and Biastoch, A.: Effects of prescribed CMIP6 ozone on simulating the Southern Hemisphere atmospheric circulation response to ozone depletion, Atmos. Chem. Phys., 21, 5777–5806, https://doi.org/10.5194/acp-21-5777-2021, 2021.

Jacob, D. J. and Winner, D. A.: Effect of climate change on air quality, Atmos. Environ., 43(1), 51–63, https://doi.org/10.1016/j.atmosenv.2008.09.051, 2009.

Jiménez, P. and Baldasano, J. M.: Ozone response to precursor controls in very complex terrains: Use of photochemical indicators to assess O_3-NO_x-VOC sensitivity in the northeastern Iberian Peninsula, J. Geophys. Res.-Atmos., 109, D20309, https://doi.org/10.1029/2004JD004985, 2004.

Lelieveld, J. and Dentener, F. J.: What controls tropospheric ozone? J. Geophys. Res., 105, 3531–3551, https://doi.org/10.1029/1999JD901011, 2000.

Levy, H.: Normal atmosphere: large radical and formaldehyde concentrations predicted, Science, 173(3992), 141-143, https://doi.org/10.1126/science.173.3992.141, 1971.

Li, J., Chen, X. S., Wang, Z. F., Du, H. Y., Yang, W. Y., Sun, Y. L., Hu, B., Li, J. J., Wang, W., Wang, T., Fu, P. Q., and Huang, H. L.: Radiative and heterogeneous chemical effects of aerosols on ozone and inorganic aerosols over East Asia, Sci. Total Environ., 622–623:1327–1342, https://doi.org/10.1016/j.scitotenv.2017.12.041, 2018.

Li, K., Jacob, D. J., Liao, H., Shen, L., Zhang, Q., and Bates, K. H.: Anthropogenic drivers of 2013-2017 trends in summer surface ozone in China, Proc. Natl. Acad. Sci. U. S. A., 116, 422–427, https://doi.org/10.1073/pnas.1812168116, 2019.

Li, M. G., Wang, L. L., Liu, J. D., Gao, W. K., Song, T., Sun, Y., Li, L., Li, X. R., Wang, Y. H., Liu, L. L., Daellenbach, K. R., Paasonen, P. J., Kerminen,V., Kulmala, M., and Wang, Y. S.: Exploring the regional pollution characteristics and meteorological formation mechanism of $PM_{2.5}$ in North China during 2013–2017, Environ. Int., 134, 105283, https://doi.org/10.1016/j.envint.2019.105283, 2020.

Lin, P. and Ming, Y.: Enhanced climate response to ozone depletion from ozone-circulation coupling, J. Geophys. Res. Atmos., 126(7), 1–14, https://doi.org/10.1029/2020jd034286, 2021.

Lin, Y. Y., Jiang, F., Zhao, J., Zhu, G., He, X. J., Ma, X. L., Li, S., Sabel, C. E., and Wang, H. K.: Impacts of O_3 on premature mortality and crop yield loss across China, Atmos. Environ, 194, 41–47, https://doi.org/10.1016/j.atmosenv.2018.09.024, 2018.

Liu, N. W., Ma, J. Z., An, X. Q., Lin, W. L., Xu, W. Y., Xu, X. B., Li, D. Q., and Li, R. P.: Source contributions and regional representativeness of surface ozone at atmospheric background stations in China, Trans. Atmos. Sci. 45(5),728–733, http://dqkxxb.cnjournals.org/dqkxxb/article/abstract/20220507?st=search (last access: 1 December 2024), 2022 (in Chinese with English abstract).

Lou, S. J., Liao, H., and Zhu, B.: Impacts of aerosols on surface-layer ozone concentrations in China through heterogeneous reactions and changes in photolysis rates, Atmos Environ., 85:123–138, http://doi.org/10.1016/j.atmosenv.2013.12.004, 2014.

Lu, X., Hong, J. Y., Zhang, L., Cooper, O. R., Schultz, M. G., Xu, X .B., Wang, T., Gao, M., Zhao,Y. H., and Zhang, Y. H.: Severe surface ozone pollution in China: a global perspective, Environ. Sci. Technol. Lett., 5, 487–494, https://doi.org/10.1021/acs.estlett.8b00366, 2018.

Lu, X., Zhang, L., Wu, T.W., Long, M. S., Wang, J., Jacob,D. J., Zhang, F., Zhang, J., Eastham, S. D., Hu, L., Zhu, L., Liu, X., and Wei, M.: Development of the global atmospheric chemistry general circulation model BCC-GEOS-Chem v1.0: Model description and evaluation, Geosci. Model Dev., 13, 3817–3838, https://doi.org/10.5194/gmd-13-3817-2020, 2020.

Maji, K. J., Ye, W. F., Arora, M., and Shiva Nagendra, S. M.: $PM_{2.5}$ related health and economic loss assessment for 338 Chinese cities, Environ. Int., 121, 392–403, https://doi.org/10.1016/j.envint.2018.09.024, 2018.

Monks, P. S., Archibald, A. T., Colette, A., Cooper, O., Coyle, M., Derwent, R., Fowler, D., Granier, C.,Law, K. S., Mills, G. E., Stevenson, D. S., Tarasova, O., Thouret, V., von Schneidemesser, E., Sommariva, R., Wild, O., and Williams, M. L.: Tropospheric ozone and its precursors from the urban to the global scale from air quality to shortlived climate forcer, Atmos. Chem. Phys., 15 (15), 8889–8973, https://doi.org/10.5194/acpd-14-32709-2014, 2015.

Morgenstern, O.: The Southern Annular Mode in 6th Coupled Model Intercomparison Project Model., J. Geophys. Res.-Atmos., 126, e2020JD034161, https://doi.org/10.1029/2020JD034161, 2021.

Neal, L. S., Dalvi, M., Folberth, G., McInnes, R. N., Agnew, P., O' Connor, F. M., Savage, N. H., and Tilbee, M.: A description and evaluation of an air quality model nested within global and regional composition-climate models using MetUM, Geosci. Model Dev., 10, 3941–3962, https://doi.org/10.5194/gmd-10-3941-2017, 2017.

Noije, T. V., Bergman, T., Sager, P. L., O'Donnell, D., Makkonen, R., Mariá Gonalves-Ageitos, Döscher, R., Fladrich, U., Hardenberg, J. V., Keskinen, J. P., Korhonen, H., Laakso, A., Myriokefalitakis, S., Ollinaho, P., García-Pando, C. P., Reerink, T., Schrödner, R., Wyser, K., and Yang, S.: Ec-earth3-aerchem: a global climate model with interactive aerosols and atmospheric chemistry participating in cmip6, Geosci. Model Dev., 14, 5637–5668, https://doi.org/10.5194/gmd-14-5637-2021, 2021.

O' Neill, B. C., Tebaldi, C., van Vuuren, D. P., Eyring, V., Friedlingstein, P., Hurtt, G., Knutti, R., Kriegler, E., Lamarque, J. F., Lowe, J., Meehl, G. A., Moss, R., Riahi, K., and Sanderson, B. M.: The Scenario Model Intercomparison Project (ScenarioMIP) for CMIP6, Geosci. Model Dev., 9, 3461–3482, https://doi.org/10.5194/gmd-9-3461-2016, 2016.

Qin, Y., Li, J. Y., Gong, K. J., Wu, Z. J., Chen,M. D., Qin,M. M., Huang, L., and Hu, J. L.: Double high pollution events in the Yangtze River Delta from 2015 to 2019: Characteristics, trends, and meteorological situations, Sci. Total Environ., 792, 148349, https://doi.org/10.1016/j.scitotenv, 2021.

Qiu, X. H., Duan, L., Chai, F. H., Wang, S. X., Yu, Q., and Wang, S. L.: Deriving high-resolution emission inventory of open biomass burning in China based on satellite observations, Environ. Sci. Technol., 50, 11779–11786, https://doi.org/10.1021/acs.est.6b02705, 2016.

Sahu, S. K., Liu, S. C., Liu, S., Ding, D., and Xing, J.: Ozone pollution in China: Background and transboundary contributions to ozone concentration & related health effects across the country, Sci.

Total Environ., 761, 144131, https://doi.org/10.1016/j.scitotenv.2020.144131, 2021.

Sellar, A. A., Jones, C .G., Mulcahy, J., Tang, Y., Yool, A., Wiltshire, A., Connor, F. M., Stringer, M., Hill, R., Palmieri, J., Woodward, S., Mora, L., Kuhlbrodt, T., Rumbold, S., Kelley, D. I., Ellis, R., Johnson, C. E., Walton, J., Abraham, N. L., Andrews, M. B., Andrews, T., Archibald, A. T., Berthou, S., Burke, E., Blockley, E., Carslaw, K., Dalvi, M., Edwards, J., Folberth, G. A., Gedney, N., Griffiths, P. T., Harper, A. B., Hendry, M. A., Hewitt, A. J., Johnson, B., Jones, A., Jones, C. D., Keeble, J., Liddicoat, S., Morgenstern, O., Parker, R. J., Predoi, V., Robertson, E., Siahaan, A., Smith, R.S., Swaminathan, R., Woodhouse, M. T., Zeng, G., and Zerroukat, M.: UKESM1: Description and evaluation of the UK Earth System Model, J. Adv. Model. Earth Syst., 11, 4513–4558, https://doi.org/10.1029/2019MS001739, 2019.

Sepulchre, P., Caubel, A., Ladant, J. B., Bopp, L., Boucher, O., Braconnot, P., Brockmann, P., Cozic, A., Donnadieu, Y., Dufresne, J. L., Estella-Perez, V., Ethé, C., Fluteau, F., Foujols, M. A., Gastineau, G., Ghattas, J., Hauglustaine, D., Hourdin, F., Kageyama, M., Khodri, M., Marti, O., Meurdesoif, Y., Mignot, J., Sarr, A. C., Servonnat, J., Swingedouw, D., Szopa, S., and Tardif, D.: IPSL-CM5A2 – an Earth system model designed for multi-millennial climate simulations, Geosci. Model Dev., 13, 3011–3053, https://doi.org/10.5194/gmd-13-3011-2020, 2020.

Shang, L., Luo, J. L., and Wang, C. X.: Ozone Variation Trends under Different CMIP6 Scenarios, Atmosphere, 12, 112, https://doi.org/10.3390/atmos12010112, 2021.

Shindell, D., Kuylenstierna, J. C. I., Vignati, E., Dingenen, R. V., Amann, M., Klimont, Z., Anenberg, S. C., Muller, N., Janssens-maenhout, G., Raes, Schwartz, J., Faluvegi, G., Pozzoli, L., Kupiainen, K., HÖglund-isaksson, L., Emberson, L., Streets, D., Ramanathan, V., Hicks, K., Oath, N. T. K., Milly, G., Williams, M., Demkine, V., and Fowler, D.: Simultaneously mitigating near-term climate change and improving human health and food security, Science, 335(6065),183–189, https://doi.org/10.1126/science.1210026, 2012.

Su, X. L., Wu, T. W., Zhang, J., Zhang, Y., Jin, J. L., Zhou, Q., Zhang, F., Liu, Y .M., Zhou, Y. M., Zhang, L., Turnock, S. T., and Furtado, K.: Present-day $PM_{2.5}$ over Asia: Simulation and uncertainty in CMIP6 ESMs, J. Meteor. Res., 36(3), 429–449, https://doi.org/10.1007/s13351-022-1202-7, 2022.

Sun, Z. and Archibal A. T.: Multi-stage Ensemble-learning-based Model Fusion for Surface Ozone Simulations: A Focus on CMIP6 Models, Environ. Sci. Technol., 8. 100124, https://doi.org/10.1016/j.ese.2021.100124, 2021.

Turnock, S. T., Allen, R. J., Andrews, M., Bauer, S. E., Deushi, M., Emmons, L., Good, P., Horowitz, L., John, J. G., Michou, M., Nabat, P., Naik, V., Neubauer, D., O' Connor, F. M., Olivié, D., Oshima, N., Schulz, M., Sellar, A., Shim, S., Takemura, T., Tilmes, S., Tsigaridis, K., Wu T. W., and Zhang J.: Historical and future changes in air pollutants from CMIP6 models, Atmos. Chem. Phys., 20, 14547–14579, https://doi.org/10.5194/acp-20-14547-2020, 2020.

Wang, C. L., Wang, Y. Y., Shi, Z. H., Sun, J. J, Gong, K. J., and Hu, J. L.: Assessment of surface ozone pollution change and its health effect in China from 2014 to2018 based on multi-source fusion data, Trans. Atmos. Sci., 44(5), 737–745, 2021, http://dqkxxb.cnjournals.org/dqkxxb/article/abstract/20210511?st=search (last access: 1 December 2024), 2021 (in Chinese with English abstract).

Wang, F. Y, Qiu X. H, Cao J. Y, Peng, L., Zhang, N. N., Yan ,Y. L., and Li, R. M.: Policy-driven changes in the health risk of $PM_{2.5}$ and O_3 exposure in China during 2013-2018, Sci. Total Environ., 757, 143775, https://doi.org/10.1016/j.scitotenv.2020.143775, 2020.

Weichenthal, S., Pinault, L. L. and Burnett, R. T.: Impact of oxidant gases on the relationship between outdoor fine particulate air pollution and nonaccidental, cardiovascular, and respiratory mortality, Sci. Rep., 7, (1), 1–10, https://doi.org/10.1038/s41598-017-16770-y, 2017.

Wesely, M. L., Cook, D. R. and Williams, R. M.: Field measurement of small ozone fluxes to snow, wet bare soil, and lake water, Bound.-Lay. Meteorol., 20, 4, 459–471, https://doi.org/10.1007/BF00122295, 1981.

Wild, O., Voulgarakis, A., O' Connor, F., Lamarque, J. F., Ryan, E. M., and Lee, L.: Global sensitivity analysis of chemistry-climate model budgets of tropospheric ozone and OH: exploring model diversity, Atmos. Chem. Phys., 20, 4047–4058, https://doi.org/10.5194/acp-20-4047-2020, 2020.

Wu, T., Zhang, F., Zhang, J., Jie, W., Zhang, Y., Wu, F., Li, L., Yan, J., Liu, X., Lu, X., Tan, H., Zhang, L., Wang, J., and Hu, A.: Beijing Climate Center Earth System Model version 1 (BCCESM1): model description and evaluation of aerosol simulations, Geosci. Model Dev., 13, 977–1005, https://doi.org/10.5194/gmd-13-977-2020, 2020.

Xiao, Q., Geng, G., Xue, T., Liu, S., Cai, C., He, K., and Zhang, Q.: Tracking $PM_{2.5}$ and O_3 Pollution and the Related Health Burden in China 2013–2020, Environ. Sci. Technol., 56, 6922–6932, https://pubs.acs.org/doi/10.1021/acs.est.1c04548, 2022.

Xie, B. and Zhang, H.: Main progresses in the research on Ozone, Sci. Tech. Eng., 14(8), 106–114, http://www.stae.com.cn/jsygc/article/abstract/1308589?st=advanced_search (last access: 1 December 2024), 2014 (in Chinese with English abstract).

Xie, F., Li, J. P., Zhang, J. K., Tian, W. S., Hu,Y. Y., Zhao, S., Sun, C., Ding, R. Q., Feng, J., and Yang,Y.: Variations in North Pacific sea surface temperature caused by Arctic stratospheric ozone anomalies, Environ. Res. Lett., 12(11), 114023, https://doi.org/10.1088/1748-9326/aa9005, 2017.

Xing, J., Wang, S., Jang, C., Zhu, Y., and Hao, J.: Nonlinear response of ozone to precursor emission changes in China: a modeling study using response surface methodology, Atmos. Chem. Phys., 11, 5027-5044, https://doi.org/ :10.5194/acp-11-5027-2011, 2011.

Xue, T., Zheng, Y. X., Geng, G. N., Xiao, Q. Y., Meng, X., Wang, M., Li, X., Wu, N. N., Zhang, Q., and Zhu, T.: Estimating Spatiotemporal Variation in Ambient Ozone Exposure during 2013-2017 Using a Data-Fusion Model, Environ. Sci. Technol., 54(23), 14877–14888, https://dx.doi.org/10.1021/acs.est.0c03098, 2020.

Yang, X.Y., Zeng, G., Iyakaremye,V., Zhu B.: Effects of different types of heat wave days on ozone pollution over Beijing-Tianjin-Hebei and its future projection. Sci. Total Environ., 2022, 837: 155762.

Yin, Z. C., Cao, B. F., and Wang, H. J.: Dominant patterns of summer ozone pollution in eastern China and associated atmospheric circulations, Atmos. Chem. Phys., 19, 13933–13943, https://doi.org/10.5194/acp-19-13933-2019, 2019.

Young, P. J., Archibald, A. T., Bowman, K. W., Lamarque, J. F., Naik, V., Stevenson, D. S., Tilmes, S., Voulgarakis, A., Wild, O., Bergmann, D., Cameron-Smith, P., Cionni, I., Collins, W. J., Dalsøren, S. B., Doherty, R. M., Eyring, V., Faluvegi, G., Horowitz, L. W., Josse, B., Lee, Y. H., MacKenzie, I. A., Nagashima, T., Plummer, D. A., Righi, M., Rumbold, S. T., Skeie, R. B., Shindell, D. T., Strode, S. A., Sudo, K., Szopa, S., and Zeng, G.: Pre-industrial to end 21st century projections of tropospheric ozone from the Atmospheric Chemistry and Climate Model Intercomparison Project (ACCMIP), Atmos. Chem. Phys., 13, 2063–2090, https://doi.org/10.5194/acp-13-2063-2013, 2013.

Young, P. J., Naik, V., Fiore, A. M., Gaudel, A., Guo, J., Lin, M. Y., Neu, J. L., Parrish, D. D., Rieder, H. E., Schnell, J. L., Tilmes, S., Wild, O., Zhang, L., Ziemke, J. R., Brandt, J., Delcloo, A., Doherty, R. M., Geels, C., Hegglin, M. I., Hu, L., Im, U., Kumar, R., Luhar, A., Murray, L., Plummer, D., Rodriguez, J., Saiz-Lopez, A., Schultz, M. G., Woodhouse, M. T. and Zeng, G.: Tropospheric Ozone Assessment Report: Assessment of global-scale model performance for global and regional ozone distributions, variability, and trends, Elem. Sci. Anth., 6, 10, https://doi.org/10.1525/elementa.265, 2018.

Yukimoto, S., Kawai, H., Koshiro, T., Oshima, N., Yoshida, K., Urakawa, S., Tsujino, H., Deushi, M., Tanaka, T., Hosaka, M., Yabu, S., Yoshimura, H., Shindo, E., Mizuta, R., Obata, A., Adachi, Y., and Ishii, M.: The meteorological research institute Earth system model O' version 2.0, MRI-ESM2.0: Description and basic evaluation of the physical component, J. Meteorol. Soc. Jpn., 97, 931–965, https://doi.org/10.2151/jmsj.2019-051, 2019.

Zhan, C. C., Xie, M., Liu, J., Wang, T. J., Xu, M., Chen, B., Li, S., Zhuang, B. L., and Li, M. M.: Surface ozone in the Yangtze River Delta, China: A synthesis of basic features, meteorological driving factors, and health impacts, J. Geophys. Res.-Atmos., 126, e2020JD033600, https://doi.org/10.1029/2020JD033600, 2021.

Zhao, S. H., Yang, X. Y., Li, Z. Q., Wang, Z. T., Zhang, Y. H., Wang, Y., Zhou, C. Y., and Ma, P. F.: Advances of ozone satellite remote sensing in 60 years, Nat. Remote Sens. Bull., 26(5), 817–833, https://doi.org/10.11834/jrs.20221632, 2022 (in Chinese with English abstract).

Zhao, S. P.,Yin, D. Y., Yu, Y., Kang, S. C., Qin, D. H., and Dong, L. X.: $PM_{2.5}$ and O_3 pollution during 2015−2019 over 367 Chinese cities: Spatiotemporal variations, meteorological and topographical impacts, Environ. Pollut., 264, 114694, https://doi.org/10.1016/j.envpol.2020.114694, 2020.

Zhang, F., Hou, C., Li, J. N., Liu, R. Q., and Liu, C. P.: A simple parameterization for the height of maximum ozone heating rate. Infrared Phys. Techn., 87, 104–112, https://doi.org/10.1016/j.infrared.2017.09.002, 2017.

Zhang, J. X., Gao, Y., Luo, K., Leung, L. R., Zhang, Y., Wang, K., and Fan, J. R.: Impacts of compound extreme weather events on ozone in the present and future, Atmos. Chem. Phys., 18, 9861–9877, https://doi.org/10.5194/acp-18-9861-2018, 2018.

Zhou T. J., Zou L. W., and Chen X. L.: Commentary on the Coupled Model Intercomparison Project Phase 6 (CMIP6), Clim. Change Res., 15 (5), 445–456, https://doi.org/10.12006/j.issn.1673-1719.2019.193, 2019 (in Chinese with English abstract).